On the dynamic stability and efficiency of centrifugal pendulum vibration absorbers with rotating pendulums

Vincent Mahé, Alexandre Renault, Aurelien Grolet, Hervé Mahé, Olivier Thomas

▶ **To cite this version:**

Vincent Mahé, Alexandre Renault, Aurelien Grolet, Hervé Mahé, Olivier Thomas. On the dynamic stability and efficiency of centrifugal pendulum vibration absorbers with rotating pendulums. Journal of Sound and Vibration, 2022, 536, pp.117157. 10.1016/j.jsv.2022.117157 . hal-03770271

HAL Id: hal-03770271
https://hal.science/hal-03770271

Submitted on 6 Sep 2022

HAL is a multi-disciplinary open access archive for the deposit and dissemination of scientific research documents, whether they are published or not. The documents may come from teaching and research institutions in France or abroad, or from public or private research centers.

L'archive ouverte pluridisciplinaire **HAL**, est destinée au dépôt et à la diffusion de documents scientifiques de niveau recherche, publiés ou non, émanant des établissements d'enseignement et de recherche français ou étrangers, des laboratoires publics ou privés.

Distributed under a Creative Commons Attribution - NonCommercial 4.0 International License

On the dynamic stability and efficiency of centrifugal pendulum vibration absorbers with rotating pendulums

V. Mahé [a,b,*], A. Renault [b], A. Grolet [a], H. Mahé [b], O. Thomas [a]

[a] *Arts et Metiers Institute of Technology, LISPEN, HESAM Université, F-59000 Lille, France*
[b] *Valeo Transmissions, Centre d'Étude des Produits Nouveaux, Espace Industriel Nord, Route de Poulainville, 80009 Amiens Cedex 1, France*

A B S T R A C T

The automotive industry uses centrifugal pendulum vibration absorbers (CPVAs) to reduce vibrations of the transmission system. These passive devices are made of several masses oscillating along a given path relative to a rotor. This work addresses a recent design of CPVA, in which the pendulums are allowed to rotate relatively to the rotor. The dynamic stability of this CPVA and the shifting of its operating point are investigated in this paper. These two aspects, crucial for an optimal vibration reduction, are assessed using an analytic dynamical model based on a perturbation method. The results obtained allow to propose new design guidelines. The validity of the model is confirmed through a comparison with a numerical resolution of the system's dynamics.

1. Introduction

In the frame of reducing polluting emissions and fuel consumption of vehicles using thermal engines, automotive manufacturers try to reduce the cylinder capacity and engine speed of rotation. These evolutions lead to a significant increase of rotation irregularities called acyclisms, mainly due to higher combustion pressure. One of the main characteristics of these reciprocating engines is the linear dependence of the acyclism frequency to the engine speed of rotation. The coefficient of proportionality is the engine order and only depends on the architecture of the engine. During an acceleration phase, the engine sweeps a wide frequency range containing some driveline torsional modes. This situation may lead to significant noise and vibration levels into the passenger compartment and premature wear of the driveline components. Centrifugal pendulum vibration absorbers (CPVAs) have been used for many years to minimise acyclisms of automotive powertrains at the engine order [1–3]. These passive devices consist of oscillating masses (pendulums) moving along particular paths relative to a primary inertia (rotor) as shown in Fig. 1. Because the pendulums are driven by the centrifugal acceleration field resulting from the rotation of the CPVA, their natural frequency is proportional to the engine speed of rotation. Hence, the CPVA acts like a classical dynamic vibration absorber [4] except that the antiresonance generated on the rotor is located at a fixed[1] order, so that the antiresonance frequency is changing linearly with the engine speed. This allows for a reduction of the vibrations over the whole engine speed range.

CPVAs exhibit nonlinearities of different natures: geometric nonlinearities due to the large amplitude of motion of the pendulums, and inertial nonlinearities, for instance due to Coriolis effects. The pendulums' path plays a key role in the nonlinear response of a CPVA. D. E. Newland showed that circular paths give the CPVA a softening behaviour, which can lead to jumps of the system's

* Corresponding author at: Arts et Metiers Institute of Technology, LISPEN, HESAM Université, F-59000 Lille, France.
E-mail addresses: vincent.mahe@ensam.eu (V. Mahé), alexandre.renault@valeo.com (A. Renault), aurelien.grolet@ensam.eu (A. Grolet), herve.mahe@valeo.com (H. Mahé), olivier.thomas@ensam.eu (O. Thomas).

[1] It is fixed in the linear regime, but it is slightly changing at large pendulum amplitudes due to nonlinear effects. This is explained later in this section.

response [5]. To avoid this jump issue, J. F. Madden recommended the use of a cycloidal path, which confers the CPVA a hardening behaviour [6]. Since the works of H. H. Denman [7], the preferred paths are epicycloids because they are the tautochronic paths of the uncoupled pendulums. The pendulums are uncoupled from the rotor when there are no acyclisms so that the rotor spins at a constant velocity and is not a degree of freedom. However, in the presence of acyclisms, the coupling between the rotor and the pendulums introduces inertial nonlinearities that play an important role in the softening/hardening behaviour of the CPVA, so that jumps of the response can still occur with an epicycloidal path [8].

Moreover, CPVAs are cyclically symmetric structures subject to nonlinear energy localisation phenomena [9,10]. This other kind of instability leads to pendulums oscillating with different phases and/or amplitudes, and it is undesired for two reasons. First, it can decrease the efficiency of the vibration reduction. Secondly, the pendulums' amplitude is limited by the cusp of their path, so that amplitude localisation can reduce the maximum torque amplitude the CPVA can filter-out. The first studies on the localisation of the pendulums' response, led by C.-P. Chao et al. [11,12], dealt with epicycloidal paths. Then, A. S. Alsuwaiyan et al. considered the case of more general paths [13]. This study on general paths was extended by S. Shaw et al., who were able to develop an accurate analytical model by taking into account the main nonlinearities coming from both the trajectory and the inertial effects [8]. B. J. Vidmar et al. investigated localisation in a CPVA made of pendulums tuned at different orders [14]. It was shown in [15–17] that the localised solutions are subjects to saddle-node bifurcations, causing jumps and Hopf bifurcations, leading to quasi-periodic solutions. K. Nishimura et al. showed that the localised response can also bifurcate towards chaotic solutions [18].

In addition to the jumps and the localisation of the response, CPVAs are subject to period-doubling bifurcations leading to a subharmonic solution [19–22]. However, those occur for excitation orders close to twice the CPVA tuning order, so they are not of interest here as this paper focuses on the response near the tuning order.

All the contributions cited above consider purely translated pendulums, probably because early works recommended to use such systems [23]. To the authors' knowledge, it is R. Chilton who first investigated the effect of pendulum rotation on the tuning order through his study of a pendulum mass rolling without slipping on a convex surface [24]. Then, R. W. Zdanowich and T. S. Wilson [25] derived the expression of the tuning order of roller-type and ring-type rotating pendulums (note that the ring-type pendulum is a special case of the monofilar pendulum investigated in [26]). A similar analysis on a pendulum linked to the rotor through a pivot was led by R. G. Mitchiner and R. G. Leonard [27]. However, it was less than ten years ago that J. Mayet and H. Ulbrich provided the first results showing that the rotational motion can significantly improve the performance of a CPVA [28–30]. In-depth studies of the rotation law of the pendulums were also led by A. Renault [31–33] and M. A. Acar [34]. Recent works by M. Cirelli, M. Cera et al. [35–39] confirmed the interest for pendulums with a rotational mobility and introduced a new way of representing the path, using curvature ratios instead of the polynomial functions used in most studies (see [13] for instance). They called "trapezoidal CPVA" systems with rotating pendulums, in opposition to "parallel CPVA", for which the pendulums' motion is a pure relative translation with respect to the rotor. X. Tan et al. considered a CPVA made of a single pendulum obeying a nonlinear rotation law and gave guidelines for the choice of this law [40]. E. R. Gomez et al. investigated theoretically and experimentally the friction losses in a CPVA with rotating pendulums [41]. In addition, they studied numerically and experimentally the behaviour of such a CPVA installed in a detailed powertrain [42]. The filtering of torsional vibrations in multi-degree-of-freedom systems using a CPVA was also investigated by K. Kadoi et al., who dealt with purely translated pendulums [43]. C. Shi et al. showed that CPVAs could be used to reduce translational vibrations and tilting in addition to torsional vibrations [44–48]. V. Mahe et al. considered the effect of rotation on a subharmonic CPVA [49,50] and on a regular CPVA [26]. Some design guidelines were given to choose the path and rotation law in order to avoid instabilities. The authors also studied the filtering effect of the pendulums responding on a localised solution and the stability of that solution [51]. Recently, J. Mayet et al. used a general framework to show how pendulums' relative rotation can increase the performance of a CPVA [52]. They assumed a unison motion of the pendulums and gave guidelines to maximise vibration reduction while avoiding jumps of the response. Other new topics of research dealing with CPVAs include precision requirement in the manufacturing process [53] and the use of double pendulums, which allows to simultaneously filter-out two orders [54].

The motivation of this paper is to investigate the dynamic stability and efficiency of a CPVA with rotating pendulums using analytical perturbation methods. The stability and performance of such systems was investigated in [29,52] without specifying a particular path nor rotation law, and in [36,38], where curvature ratios and a rolling radius were used to describe the path and rotation law. In the present paper, it is chosen to represent the path and rotation law using polynomial functions of the pendulums' positions, like in [26,31–34]. This representation gives a clear physical meaning to the coefficients of those polynomials, which are the parameters that control the linear and nonlinear tuning of the CPVA. In addition, this representation allows designers to easily adjust the tuning in practice as one simply has to change the value of the polynomial coefficients. The analytical model developed in this paper uses different assumptions than those of [26], which allows to capture the nonlinearities arising from inertial terms, hence making the model more accurate. The efficiency of a CPVA is closely related to the features of the antiresonance generated by the pendulums on the rotor. If the rotor's amplitude at the antiresonance is low and the antiresonance order does not shift much as the torque amplitude is increased, the CPVA will significantly reduce the vibrations over the whole torque range. D. E. Newland observed early on that the antiresonance order generated by bifilar pendulums following a circular path diminishes as the torque amplitude is increased [55]. This shifting of the operating point for circular path pendulums was also studied by M. Sharif-Bakhtiar et al. [56] and observed experimentally by A. G. Haddow [57]. Over-tuning the pendulums was recommended to minimise the decrease in performance due to the antiresonance shifting, but it is limited by the occurrence of jumps of the system's response [55,56]. A. Renault proposed a procedure to track the locus of the antiresonance and applied his method to Euler's pendulum [58]. He observed that the antiresonance does not necessarily shift in the same direction as the resonance of the system. This is of great importance for CPVAs and will be investigated in this paper.

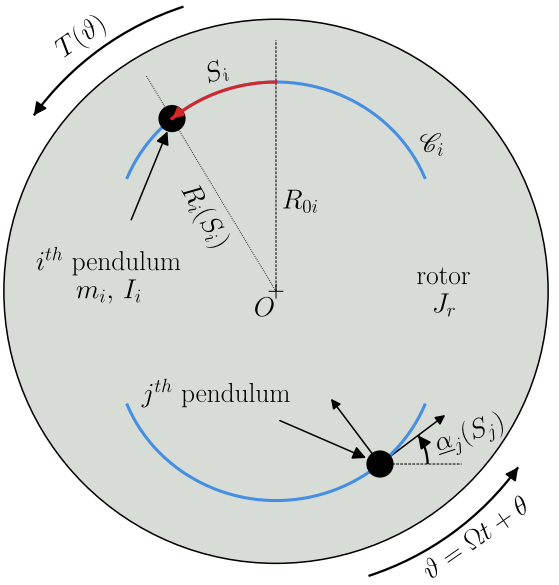

Fig. 1. Representation of the system studied. It is made of $N = 2$ pendulums.

This paper is organised as follows. Section 2 describes the modelling of the CPVA and presents a linear analysis. The response of a CPVA and its stability are derived in Section 3. Case studies and design guidelines allowing to reduce the shifting of the antiresonance and to avoid instabilities are presented in Section 4. This paper ends with a conclusion in Section 5.

2. Modelling and linear analysis

2.1. Modelling

The system studied is shown in Fig. 1. A rotor of inertia J_r rotates about its centre O. Its total angular position is $\vartheta(t) = \Omega t + \theta(t)$ where t is the time, Ω is the mean rotational velocity and $\theta(t)$ corresponds to the fluctuating part of the rotation. A torque $T(\vartheta) = T_0 + T_\theta(\vartheta)$ is applied to the rotor where T_0 is its constant part and $T_\theta(\vartheta)$ is periodic. At equilibrium, $T_0 = b_r\Omega$ where b_r is the linear viscous damping coefficient of the rotor, such that the constant torque balances with the damping to set the mean rotational speed Ω. N pendulums of mass m_i and inertia I_i (about their centre of mass) oscillate on their path $\mathscr{C}_i$. Their position on these paths is given by the curvilinear abscissa $S_i(t)$ and their distance from O is $R_i(S_i)$. The characteristic dimension $R_{0i} = R_i(S_i = 0)$ is the distance between O and the vertex of the path. In addition to the traditional translation motion, the present study considers that the pendulums rotate about their centre of mass according to the rotation function $\underline{\alpha}_i(S_i)$. As for the rotor, an equivalent linear viscous damping coefficient b_i is used to model the damping between the ith pendulum and the rotor. In the later, pendulums and their associated path and rotation functions will be considered identical so that subscript "i" will be dropped when addressing pendulums' parameters.

In order to write the equations of motion in a non-dimensional form, the following parameters and variables are introduced:

$$
\begin{gathered}
s_i = \frac{S_i}{R_0}, \quad y = \frac{\dot{\vartheta}}{\Omega} = 1 + \frac{\dot{\theta}}{\Omega}, \quad \eta = \frac{I}{mR_0^2}, \quad \mu = \frac{NmR_0^2}{J_r + NI}, \quad \bar{b} = \frac{b}{m\Omega}, \quad \bar{b}_r = \frac{b_r}{(J_r + NI)\Omega}, \\
\bar{T}(\vartheta) = \bar{T}_0 + \bar{T}_\theta(\vartheta) = \frac{T(\vartheta)}{(J_r + NI)\Omega^2}, \quad x(s_i) = \frac{R(R_0 s_i)^2}{R_0^2}, \quad z(s_i) = \sqrt{x(s_i) - \frac{1}{4}\left(\frac{dx(s_i)}{ds_i}\right)^2}, \\
\alpha(s_i) = \underline{\alpha}(R_0 s_i), \quad \gamma(s_i) = \frac{d\alpha(s_i)}{ds_i},
\end{gathered}
\tag{1}
$$

where $(\dot{\bullet}) = \partial(\bullet)/\partial t$. The s_i and y are the $N + 1$ degree-of-freedom of the system. They correspond to the dimensionless relative position of the pendulums and rotational velocity of the rotor, respectively. η and μ are inertia ratios, $\bar{b}$ and $\bar{b}_r$ are non-dimensional damping constants and $\bar{T}(\vartheta)$ is the non-dimensional torque applied on the rotor. $x(s_i)$ and $z(s_i)$ are path functions while $\alpha(s_i)$ and $\gamma(s_i)$ are rotation functions. In this paper, $x(s_i)$ and $\alpha(s_i)$ are written as polynomials in the curvilinear abscissa s_i such that

$$
x(s_i) = 1 - n_t^2 s_i^2 + \sum_{k=3}^{N_x} x_{[k]} s_i^k, \quad \alpha(s_i) = \sum_{k=0}^{N_\alpha} \alpha_{[k]} s_i^k,
\tag{2}
$$

where n_t is the order of the pendulums' path and $x_{[k]}$, $\alpha_{[k]}$ are path and rotation coefficients. In the special case $x_{[k]} = 0, \forall k$, the pendulums' path are epicycloids of order n_t, which are the tautochronic paths when the rotor spins at a constant speed [7]. Note that paths defined as in Eq. (2) have a cusp point [7]. For small $x_{[k]}, \forall k$, the cusp point can be approximated by the cusp of the epicycloid, given by

$$s_{\text{cusp}} = \frac{1}{n_t\sqrt{1+n_t^2}}. \tag{3}$$

In order to give $\bar{T}(\vartheta)$ the meaning of an external forcing term, we replace the independent variable t by the rotor's position ϑ [59], which can be seen as a non-dimensional time. Using the chain rule, one can show that

$$\dot{(\bullet)} = \Omega y(\bullet)', \quad \ddot{(\bullet)} = \Omega^2 yy'(\bullet)' + \Omega^2 y^2(\bullet)'', \tag{4}$$

where $(\bullet)' = \partial(\bullet)/\partial\vartheta$ (the details can be found in [49]). Hence, the non-dimensional rotor's acceleration is now $\ddot{\vartheta}/\Omega^2 = \dot{y}/\Omega = yy'$. Using the non-dimensional quantities (1) and the chain rule (4), one can write the equations of motion as

$$\frac{1}{N}\left[\sum_{i=1}^{N}(N+\mu x(s_i))yy' + \mu\left(z(s_i)+\eta\gamma(s_i)\right)(yy's_i' + y^2s_i'') + \mu y^2 s_i'\left(\frac{dx(s_i)}{ds_i} + \frac{dz(s_i)}{ds_i}s_i' + \eta\frac{d\gamma(s_i)}{ds_i}s_i'\right)\right] + \bar{b}_r y = \bar{T}(\vartheta), \tag{5a}$$

$$\left[z(s_i)+\eta\gamma(s_i)\right]y' + \left[1+\eta\gamma(s_i)^2\right](y's_i' + ys_i'') + \eta\gamma(s_i)\frac{d\gamma(s_i)}{ds_i}ys_i'^2 - \frac{1}{2}\frac{dx(s_i)}{ds_i}y + \bar{b}s_i' = 0, \qquad i = 1,\dots,N. \tag{5b}$$

Computation details can be found in [49]. Eq. (5a) governs the motion of the rotor while the N Eqs. (5b) govern the motion of the pendulums.

From now on, it is assumed that the fluctuating torque applied on the rotor contains only one harmonic whose non-dimensional form is $\bar{T}_1\cos(n\vartheta)$, where n is the excitation order. For a car engine, n corresponds to the number of strikes per revolution of the crankshaft.

2.2. Linear analysis

First of all, one can use Eq. (4) to show that, at first order, $1+\theta' \approx y$ and $\theta'' \approx yy' \approx y'$ (the demonstration can be found in [49]). Hence, it is possible to represent the motion of the rotor with position θ instead of velocity y. This way, all the degree-of-freedom of the system are positions, which facilitates the representation of the mode shapes. Using θ instead of y and the balance between the constant torque and the damping $\bar{b}_r = \bar{T}_0$ (*cf.* Section 2.1), one can linearise Eqs. (5a) and (5b). This leads to the free, conservative, linear equations

$$(1+\mu)\theta'' + \frac{\mu\Lambda_c}{N}\sum_{i=1}^{N}s_i'' = 0, \tag{6a}$$

$$\Lambda_c\theta'' + \Lambda_m s_i'' + n_t^2 s_i = 0, \quad i = 1,\dots,N. \tag{6b}$$

Λ_m and Λ_c are constants representing the equivalent mass of a pendulum due to the effect of the rotatory inertia and the linear coupling term between a pendulum and the rotor, respectively. They are given by

$$\Lambda_m = 1+\eta\alpha_{[1]}^2, \quad \Lambda_c = 1+\eta\alpha_{[1]}, \tag{7}$$

where $\alpha_{[1]}$ is the linear rotation coefficient (*cf.* Eq. (2)).

The linearised equations of motions (6) can be written as a matrix equation. Solving the associated eigenvalue problem requires to find the eigenvalues of an arrowhead matrix whose diagonal terms are all identical except for the first one. As explained in [60], the eigenvalues of such a matrix are those of a reduced 2×2 matrix together with the identical terms of the diagonal. Applying this procedure, one can find that the eigenorders and mode shapes of the system are

$$\begin{aligned}
&n_{00} = 0, \quad n_{10} = n_p, \quad n_{20} = n_p\sqrt{\frac{1+\mu}{1+\mu\left(1-\frac{\Lambda_c^2}{\Lambda_m}\right)}}\\
&\boldsymbol{\phi_{00}} = [1,0,\dots,0]^\intercal, \quad \boldsymbol{\phi_{20}} = \left[-\frac{\mu\Lambda_c}{1+\mu},1,\dots,1\right]^\intercal,\\
&\boldsymbol{\phi_{10}}_i[i+1] = -\boldsymbol{\phi_{10}}_i[i+2] = 1, \quad \boldsymbol{\phi_{10}}_i[j\neq\{i+1,i+2\}] = 0, \quad i = 1,\dots,N-1.
\end{aligned} \tag{8}$$

The eigenorders can be seen as non-dimensional eigenfrequencies and superscript $^\intercal$ indicates the transpose. n_p is the pendulums' tuning order, which is related to the path order n_t such that

$$n_p = \frac{n_t}{\sqrt{\Lambda_m}}, \tag{9}$$

and it corresponds to the eigenorder of the pendulums when they are uncoupled from the rotor. The value inside the brackets after $\boldsymbol{\phi_{10}}_i$ is used to refer to one of its components.

$(n_{00}, \boldsymbol{\phi_{00}})$ is a rigid body mode for which only the rotor is excited. $\left(n_{10}, \boldsymbol{\phi_{10_i}}\right)$ are $N-1$ degenerated modes for which two pendulums are moving in phase-opposition. Their eigenvalue n_{10} has multiplicity $N-1$ and the rotor is a node of these modes. For a CPVA made of only two pendulums, $(n_{10}, \boldsymbol{\phi_{10}})$ is not degenerated and simply represents a phase-opposition motion of the pendulums. $(n_{20}, \boldsymbol{\phi_{20}})$ is a mode for which the pendulums move in unison but in phase-opposition with respect to the rotor (provided that $\Lambda_c > 0$, which is the case for reasonable parameters). It will be referred-to as the "unison mode" or "mode 2". To filter-out a fluctuating torque, one typically chooses $n_p \approx n$ to generate an antiresonance on the rotor at $n_{AR} \approx n_p$ using the unison mode.

Note that in the case of a real automotive driveline (a simple model of which consists in successive rotors linked through torsional springs [61]), the CPVA should be placed as close as possible from the source of excitation (i.e. the engine). Doing so, the antiresonance generated by the pendulums exists on every driveline components located after the CPVA [62], which allows to isolate the whole driveline from the torque fluctuations.

3. Response and stability of the CPVA

3.1. Scaling and simplification of the equations

The first step to derive approximate analytical solutions of Eqs. (5a) and (5b) is to simplify those equations. The full procedure is detailed in [49], so only the main steps are reminded here. The path and rotation functions followed by the pendulums, whose general form are given by Eq. (2), are chosen to be

$$x(s_i) = 1 - n_t^2 s_i^2 + x_{[4]} s_i^4, \quad \alpha(s_i) = \alpha_{[1]} s_i + \alpha_{[3]} s_i^3, \tag{10}$$

and the rotor's rotational velocity is expanded such that

$$y(\vartheta) = 1 + y_\theta(\vartheta). \tag{11}$$

Following S. Shaw et al. [8], we assume small damping, small fluctuations of the rotor's rotational velocity, small external torque amplitudes, small ratio of the pendulums' geometric inertia over the CPVA's inertia and a path close to an epicycloid. In addition, we assume a rotational law close from a linear one. Hence, we can scale the parameters such that

$$\bar{b} = \epsilon\tilde{b}, \quad \bar{b}_r = \epsilon\tilde{b}_r, \quad \bar{T}_1 = \epsilon\tilde{T}_1, \quad \mu = \epsilon\tilde{\mu}, \quad y_\theta = \epsilon\tilde{y}_\theta, \quad \theta' = \epsilon\tilde{\theta}', \quad x_{[4]} = \epsilon\tilde{x}_{[4]}, \quad \alpha_{[3]} = \epsilon\tilde{\alpha}_{[3]}, \tag{12}$$

where ϵ is a small parameter that can for instance be chosen to be μ. In the following, only first-order terms will be retained in the rotor's equation. Hence, like in Section 2.2, the approximation $\tilde{\theta}' \approx \tilde{y}_\theta$ can be used in order to represent the degree-of-freedom of the rotor through its position rather than its velocity [49].

Using Eqs. (10), (11) and (12) and Taylor series for $z(s_i)$, Eqs. (5a) and (5b) can be simplified such that

$$\tilde{\theta}'' = \frac{\tilde{\mu}}{N}\left[\sum_{i=1}^{N} n_p^2 \Lambda_c s_i + 2n_t^2 s_i s_i' + n_t^2(1+n_t^2)\left(s_i s_i'^2 - \frac{n_p^2}{2} s_i^3\right)\right] + \tilde{T}_1 \cos(n\theta), \tag{13a}$$

$$\begin{aligned} s_i'' + n_p^2 s_i = -\epsilon\Lambda_m^{-1} \Bigg\{ & \frac{\Lambda_c^2\tilde{\mu}}{N}\sum_{j=1}^{N} n_p^2 s_j + \tilde{b} s_i' + \frac{\tilde{\mu} n_t^2 \Lambda_c}{N}\left[\sum_{j=1}^{N} s_j(2s_j' + s_i')\right] \\ & + \frac{\tilde{\mu} n_t^2}{N}\left[\sum_{j=1}^{N}(1+n_t^2)\Lambda_c\left(s_j s_j'^2 - \frac{n_p^2}{2}(s_j^3 + s_j s_i^2)\right) + 2\Lambda_m s_j s_j' s_i'\right] \\ & + 6\eta\alpha_{[1]}\tilde{\alpha}_{[3]}(s_i s_i'^2 + s_i^2 s_i'') - 2\tilde{x}_{[4]} s_i^3 + \left(\Lambda_c + \Lambda_m s_i' - \frac{n_t^2(1+n_t^2)}{2} s_i^2\right)\tilde{T}_1 \cos(n\vartheta) \Bigg\}, \quad i = 1, \ldots, N. \end{aligned} \tag{13b}$$

Eq. (13a) expresses the rotor's acceleration as a function of the pendulums' motion. The first, second and third terms are linear, quadratic and cubic in s_i, respectively. The pendulums' equations (13b) are uncoupled from the rotor's dynamics, so that one can solve them to obtain the s_i and then inject the results in Eq. (13a) to retrieve the rotor's response. Eqs. (13b) contain the effect of the external torque, the damping, the coupling between pendulums (both linear and nonlinear) through the sums over N, and the perturbations of the path and rotation functions. Eqs. (13b) are weakly coupled because pendulums are coupled indirectly through the rotor and their effect on the rotor is small as their relative inertia is small [21]. These equations are also weakly nonlinear because the path and rotation functions chosen are close to an epicycloid and a linear rotation (indeed, $x_{[4]}$ and $\alpha_{[3]}$ were assumed to be of order ϵ, *cf.* Eq. (12)), which render a quasi-linear behaviour for small fluctuations of the rotational speed.

3.2. Solutions of the simplified equations

The method of multiple scales [63] is used to find the solutions of Eqs. (13b). Two rotation scales are introduced, $\vartheta_0 = \vartheta$ and $\vartheta_1 = \epsilon\vartheta$, and pendulums coordinates are expanded such that

$$s_i(\vartheta) = s_{i1}(\vartheta_0, \vartheta_1) + \epsilon s_{i2}(\vartheta_0, \vartheta_1). \tag{14}$$

As the excitation order n is close from n_p, it is convenient to define the detuning term σ as

$$n = n_p + \epsilon\sigma. \tag{15}$$

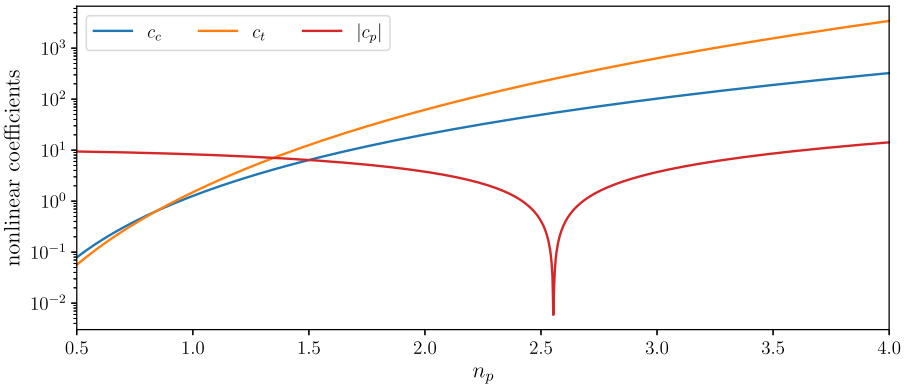

Fig. 2. Evolution of the nonlinear coefficients c_c, c_t and c_p as a function of the tuning order n_p. The other parameters are given in Table 1.

$\sigma > 0$ and $\sigma < 0$ correspond to under-tuned and over-tuned pendulums, respectively. Applying the method of multiple scales yields first-order solutions of the form

$$s_{i1}(\vartheta_0, \vartheta_1) = a_i(\vartheta_1)\cos\left(n\vartheta_0 - \xi_i(\vartheta_1)\right). \tag{16}$$

Amplitudes a_i and phases ξ_i are governed by the system

$$\begin{cases} D_1 a_i &= f_{a_i}(\boldsymbol{a}, \boldsymbol{\xi}), \ \text{(a)} \\ a_i D_1 \xi_i &= f_{\xi_i}(\boldsymbol{a}, \boldsymbol{\xi}), \ \text{(b)} \end{cases} \tag{17}$$

where $D_1(\bullet) = \partial(\bullet)/\partial\vartheta_1$ and $\boldsymbol{a}, \boldsymbol{\xi}$ are vectors containing the a_i and ξ_i, respectively. Functions f_{a_i} and f_{ξ_i} are given in Appendix A. The solutions sought are those at steady-state, meaning that the amplitudes and phases are invariant with ϑ such that

$$D_1 a_i = D_1 \xi_i = 0, \quad \forall i. \tag{18}$$

Moreover, we look for a response of the pendulums on the unison mode, which implies

$$a_i = a, \quad \xi_i = \xi, \quad \forall i. \tag{19}$$

The pendulums' response is obtained by introducing the steady-state (18) and unison (19) conditions in system (17) and solving for σ, $\tilde{T}_1$ and ξ. The solutions obtained are given in Appendix B. For readability, it is convenient to introduce the nonlinear coefficients

$$\begin{aligned} &c_2 = -c_c + 2c_t + c_p, \quad c_c = \tilde{\mu} n_t^4, \\ &c_t = \frac{\Lambda_c}{2}\tilde{\mu} n_p^2 n_t^2 (1 + n_t^2), \quad c_p = 3(\tilde{x}_{[4]} + 2n_p^2 \eta \alpha_{[1]} \tilde{\alpha}_{[3]}). \end{aligned} \tag{20}$$

c_2 is the nonlinear coefficient governing the hardening/softening behaviour of mode 2 (i.e. the unison mode). c_c, c_t and c_p are nonlinear coefficients related to Coriolis effects, the large displacements along the path, and the perturbation of the path and rotation functions, respectively. The backbone curve of the unison mode is obtained by cancelling the damping and forcing in the forced order response (*cf.* Eq. (B.1a)), leading to

$$n_2 = n_p + \frac{\Lambda_c^2 n_p^2 \mu}{2\Lambda_m n_p} - \epsilon \frac{c_2}{4\Lambda_m n_p} a^2. \tag{21}$$

n_2 is the resonance order of mode 2. It is interesting to note that even with an epicycloidal path and a linear rotation law (i.e. $c_p = 0$), the behaviour of mode 2 is hardening or softening, depending on the sign of $c_c - 2c_t$ (*cf.* Eq. (20)). These two coefficients are due to the nonlinear coupling between the rotor and pendulums, and their presence shows that the epicycloid is the tautochronic path of the pendulums only if they are uncoupled from the rotor. This was previously remarked by H. H. Denman [7]. Moreover, for reasonable parameters and tuning orders larger than 1, we have $2c_t > c_c > 0$ (*cf.* Fig. 2), so that the unison mode is typically softening. One can choose c_p to increase (decrease) this softening behaviour, resulting in softened (hardened) pendulums. Hence, c_p can be seen as the nonlinear tuning parameter of the CPVA while n_p is the linear tuning parameter. Note that c_c and c_t depend linearly on μ. Hence, for small values of μ, c_p dominates so that only small negative c_p values yield a hardening behaviour. c_c, c_t and c_p also depend on n_p, as illustrated in Fig. 2. It is very interesting to realise that for small n_p values, the contribution of c_c and c_t is negligible, even for reasonable μ values. Small n_p values can be encountered when dealing with cylinder deactivation, in which case a model simpler than the one presented in this paper can be used [26].

The response of the first three harmonics of the rotor's acceleration are obtained by substituting the pendulums' solutions in Eq. (13a). Their amplitude and phase are given in Appendix B.

3.3. Stability analysis

The procedure to determine the stability is the same as that used in [26], so only the main steps are reminded here. First, system (17) is rewritten as

$$\begin{cases} D_1 a_i = f_{a_i}(\boldsymbol{a}, \boldsymbol{\xi}), & \text{(a)} \\ D_1 \xi_i = f^*_{\xi_i}(\boldsymbol{a}, \boldsymbol{\xi}), & \text{(b)} \end{cases} \tag{22}$$

where we define $f^*_{\xi_i} = f_{\xi_i}/a_i$. Then, the Jacobian $\boldsymbol{J}$ of system (22) is computed and evaluated on the unison solution at steady state. $\boldsymbol{J}$ is a block-circulant matrix of size $2N \times 2N$ such that

$$\boldsymbol{J} = \begin{bmatrix} \boldsymbol{J_1} & \boldsymbol{J_2} & \cdots & \boldsymbol{J_2} \\ \boldsymbol{J_2} & \ddots & \ddots & \vdots \\ \vdots & \ddots & \ddots & \boldsymbol{J_2} \\ \boldsymbol{J_2} & \cdots & \boldsymbol{J_2} & \boldsymbol{J_1} \end{bmatrix}, \quad \boldsymbol{J_1} = \begin{bmatrix} \dfrac{\partial f_{a_i}}{\partial a_i} & \dfrac{\partial f_{a_i}}{\partial \xi_i} \\ \dfrac{\partial f^*_{\xi_i}}{\partial a_i} & \dfrac{\partial f^*_{\xi_i}}{\partial \xi_i} \end{bmatrix}, \quad \boldsymbol{J_2} = \begin{bmatrix} \dfrac{\partial f_{a_i}}{\partial a_j} & \dfrac{\partial f_{a_i}}{\partial \xi_j} \\ \dfrac{\partial f^*_{\xi_i}}{\partial a_j} & \dfrac{\partial f^*_{\xi_i}}{\partial \xi_j} \end{bmatrix}. \tag{23}$$

$\boldsymbol{J_1}$ represents the effect of a perturbation of the ith pendulum on itself, while $\boldsymbol{J_2}$ represents the effect of a perturbation of the jth pendulum on the ith one with $i \neq j$. The unison solution is subjected to a jump of the response if $\det[\boldsymbol{J_1} + (N-1)\boldsymbol{J_2}] < 0$, and it is subjected to localisation if $\det[\boldsymbol{J_1} - \boldsymbol{J_2}] < 0$ [26,64]. The limits of those instability regions define two bifurcation curves, which represent the bifurcation points of the unison solution for every forcing amplitude. The bifurcations leading to a jump are saddle-node bifurcations, hence the associated bifurcation curve is called a_{sn}. The other curve is called a_{pf} as localisation arises through a pitchfork bifurcation. Each crossing between a and a_{sn} or a_{pf} leads to a change of stability of the unison solution. The expression of the bifurcation curves is given in Appendix C under the form $\sigma_{sn}(a)$ and $\sigma_{pf}(a)$.

4. Case studies and design guidelines

The aim here is to present the main assets of the analytical model and to assess the accuracy of this model by comparing it to numerical resolutions of the initial equations of motion (5a) and (5b). These equations will be solved numerically using MANLAB, which is a path-following and bifurcation analysis software [65,66].

4.1. Response of the CPVA as a function of linear mistuning

In practice, the excitation order is fixed such that n is a constant. However, pendulums may not be tuned exactly to the excitation. This mistuning can be intentional or may arise from material imperfections. Either way, varying the excitation order is similar to introducing mistuning (provided that pendulums are equally mistuned) and is therefore relevant for studying the effect of mistuning on the system's response [17].

The order response of pendulums at unison and their stability is shown in Fig. 3 for several torque amplitudes. The bending of the response to the left indicates that pendulums exhibit a softening behaviour. The unison response computed analytically (green curves) fits quite well with the numerical results (green lines with square markers). There are however discrepancies at large amplitudes and at the resonance. At large amplitudes, the behaviour is more hardening than expected for $n < 1.56$ and more softening for $n > 1.56$. The amplitude at the resonance is not well estimated, but this was to be expected for two reasons. First, the analytical method uses a perturbation around $n = n_p$, which is not close from the resonance. Secondly, the system has very small damping, making the amplitude at the resonance difficult to predict accurately. Note that the analytical solutions above s_{cusp} exist only because of the use of Taylor series to approximate $z(s_i)$ in Section 3.1, so they are not physically relevant. The unstable zones leading to localisation (red) and jumps (blue) are shown. Each crossing between the unison solution and the limit of those zones leads to a change of stability. This is verified by MANLAB results, which indicate stability changes with red and blue stars. The position of the unstable zones is quite accurate as their limits fit well with the stars. Finally, note that Eq. (3) is a good approximation of the cusp of the path as it almost corresponds to the maximum amplitude that can be computed with numerical methods.

Fig. 4 displays the rotor's response associated to the pendulums' response shown in Fig. 3. Again, the overall response and its stability are well predicted, though discrepancies arise at large amplitudes. The strange shape of the response around the resonance for $\bar{T}_1 > 0.005$ can simply be ignored as it occurs for pendulums way above their cusp, which is non-physical. The zoom included in the figure allows to better see the evolution of the antiresonance with $\bar{T}_1$. For low torque amplitudes, the antiresonance order is $n_{AR} \approx n_p$, but as $\bar{T}_1$ is increased, n_{AR} shifts to the right. It is interesting to note that contrarily to the antiresonance, the resonance is shifting to the left, so the softening/hardening behaviour of the antiresonance is completely different from that of the resonance. This was previously observed for Euler's pendulum by A. Renault et al. [58] and is investigated further in the next section. One can see in the zoom in Fig. 4 that the antiresonance gets narrower as $\bar{T}_1$ is increased (this is because the amplitude at the antiresonance remains very small over the whole torque range, while the rest of the response considerably increase with $\bar{T}_1$). This makes n_{AR} harder to predict for large $\bar{T}_1$ values, as seen in the zoom in Fig. 4 for $\bar{T}_1 = 0.075$.

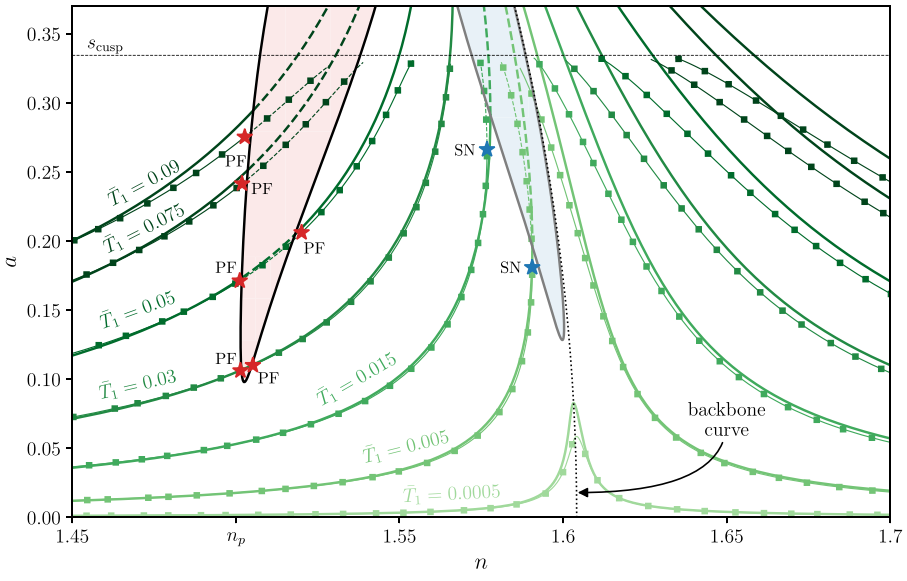

Fig. 3. Order response of the pendulums for several torque amplitudes. The analytical results representing the pendulums' response at unison are represented as green lines. The darker the line the larger the associated torque amplitude. For each analytical response there is an associated numerical result, computed with MANLAB, shown as a green line with square markers. Dashed lines indicate unstable solutions. The unstable zones obtained analytically are coloured in red (associated to localisation) and blue (associated to the jumps). Bifurcation points are also computed with MANLAB. Pitchfork and saddle-node bifurcations are represented as red and blue stars, respectively. The cusp of the path, approximated using Eq. (3), is shown as a black dashed line. The backbone curve of the unison mode is the black dotted line. The parameters of the CPVA are given in Table 1. (For interpretation of the references to colour in this figure legend, the reader is referred to the web version of this article.)

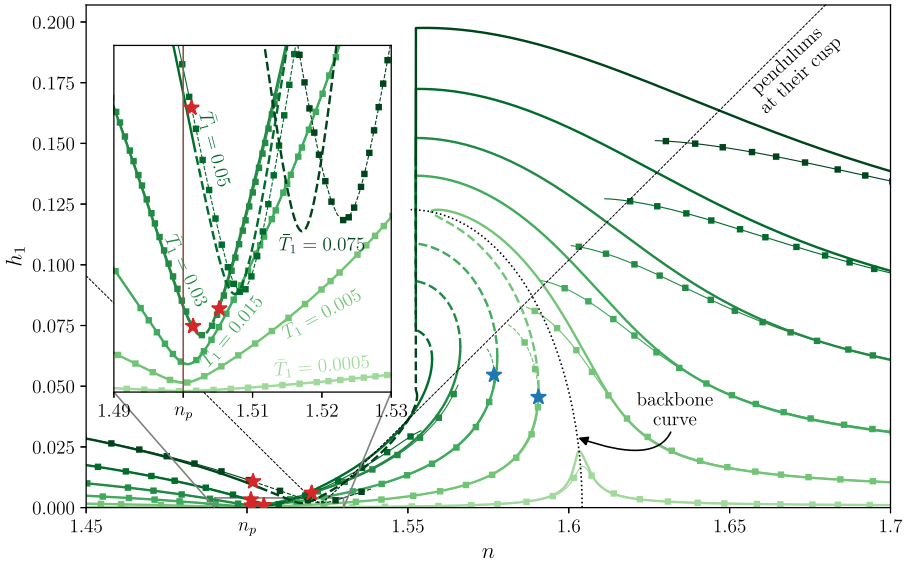

Fig. 4. Order response of the rotor for several torque amplitudes. The associated pendulums' response is given in Fig. 3 (however, for clarity, the curve corresponding to $\bar{T}_1 = 0.09$ is not shown in the present figure). The analytical results representing the pendulums' response at unison are represented as green lines. The darker the line the larger the associated torque amplitude. For each analytical response there is an associated numerical result, computed with MANLAB, shown as a green line with square markers. Dashed lines indicate unstable solutions. Pitchfork and saddle-node bifurcations computed with MANLAB are represented as red and blue stars, respectively. The value of h_1 for which the pendulums reach their cusp is shown as a black dashed line. It is computed using Eqs. (3), (B.1b) and (B.2a). The backbone curve of the unison mode is the black dotted line. A zoom around the antiresonance is included in the figure. The parameters of the CPVA are given in Table 1. (For interpretation of the references to colour in this figure legend, the reader is referred to the web version of this article.)

Table 1
Parameters of the CPVA studied in this section.

N	n_p	η	μ	$x_{[4]}$	$\alpha_{[1]}$	$\alpha_{[3]}$	$\bar{b}$	$\bar{b}_r$
2	1.5	0.5	0.1	−0.2	0.5	−0.1	0.005	0.008

4.2. Antiresonance locking

The filtering is optimal if the excitation order n coincides with the antiresonance order n_{AR} over the whole torque range. However, as seen in the previous section, nonlinear effects cause n_{AR} to be amplitude-dependent, so it is crucial to assess its evolution to ensure the CPVA achieves good performance over the whole torque range. The analytical model can be used to obtain a design rule minimising the shift of the antiresonance so it remains close from n_p. The procedure is described below.

The rotor's acceleration can be approximated by

$$\theta'' = h_1\cos(n\vartheta - \psi_1) + h_2\cos(2n\vartheta - \psi_2) + h_3\cos(3n\vartheta - \psi_3), \tag{24}$$

where the harmonics' amplitudes h_i and phases ψ_i $(i = 1, 2, 3)$ are given in Appendix B. Neglecting the effect of damping and considering excitation orders smaller than the order at resonance, the pendulums are in phase-opposition with the external torque so that $\cos(\xi) = -1$. Using this in Eq. (B.2a) leads to the expression of the amplitude of the rotor's first harmonic

$$h_1 = \left|\bar{T}_1 - \mu n_p^2\Lambda_c a - \frac{\mu(2n^2 - 3n_p^2)n_t^2(1 + n_t^2)}{8}a^3\right|. \tag{25}$$

Using Eq. (B.1b) to perform a Taylor series of $\bar{T}_1$ in a leads to

$$\tilde{T}_1 = a\left|\Lambda_c\tilde{\mu}n_p^2 - \frac{2\Lambda_m n_p\sigma}{\Lambda_c} + \left(\frac{3c_t - 2c_2}{4\Lambda_c} - \frac{3\Lambda_m n_p c_f\sigma}{4\Lambda_c^2}\right)a^2\right| + \mathcal{O}(a^4), \tag{26}$$

where c_f is a nonlinear coefficient representing the nonlinear forcing on the pendulums (*cf.* Appendix A). It is defined as

$$c_f = n_t^2(1 + n_t^2). \tag{27}$$

In Eq. (26), the term inside the absolute value can fairly be assumed positive as $\mu\Lambda_c n_p^2$ is positive for reasonable parameters, a^2 is negligible for small values of a, σ is assumed small and $\bar{T}_1$ increases monotonically with a if there is no jump. Introducing Eq. (26) in Eq. (25) leads to

$$h_1 = \frac{a}{2\Lambda_c}\left|4\Lambda_m n_p\sigma + \left(\frac{3\Lambda_m n_p c_f\sigma}{2\Lambda_c} + c_2 - 2c_t\right)a^2\right|. \tag{28}$$

Because there is no damping in our reasoning, the amplitude of the rotor's first harmonic must be null at the antiresonance. Hence, the antiresonance locus is obtained by solving $h_1 = 0$ for σ, leading to

$$n_{AR} = n_p + \epsilon\frac{c_c - c_p}{4\Lambda_m n_p}a^2 + \mathcal{O}(a^4). \tag{29}$$

Thus, the condition to lock the antiresonance at n_p is

$$c_p = c_c > 0. \tag{30}$$

It is of great importance to note that rule (30) is different from the one rendering a tautochronic response of the pendulums. Indeed, one can see from Eq. (21) that the condition yielding a constant value of n_2 is

$$c_2 = 0 \Leftrightarrow c_p = c_c - 2c_t. \tag{31}$$

Rule (30) also requires the pendulums' path not to be the tautochronic path of the uncoupled system (this would correspond to $c_p = 0$, *cf.* Appendix D). Hence, despite the large focus on tautochronic designs [28,38,67,68], these are not the preferred ones. This highlights the importance of studying the antiresonance locus and not only the pendulums' response.

Fig. 5 shows the response of a CPVA tuned to fulfil condition (30). The rotor's response (b) is very well predicted by the model up to $\bar{T}_1 = 0.03$. For $\bar{T}_1 = 0.05$, the analytical model predicts a small shift of the antiresonance to the left while MANLAB shows that it actually shifts to the right. This shifting is amplified for $\bar{T}_1 = 0.075$, which highlights limits of the analytical model.

Looking at the pendulums' response (a), one can clearly see the softening behaviour for $\bar{T}_1 = 0.03$, with a jump at $n = 1.544$. However, at higher torque amplitudes, the MANLAB solutions show that the behaviour becomes less softening. Moreover, for $\bar{T}_1 = 0.075$, there are two pitchfork bifurcations that are not predicted by the analytical model. This confirms that the accuracy of the model is limited to small torque amplitudes. Note also that even though rule (30) requires a softening behaviour, it is much less softening than for a circular path. Indeed, in the case presented in Fig. 5, $x_{[4]} = 0.3261$, while for the same parameters but a circular path, $x_{[4]} = 2.6303$ [13]. Moreover, values of $\eta\alpha_{[1]}\alpha_{[3]}$ larger than those given in Table 1 would require smaller values of $x_{[4]}$ to fulfil rule (30).

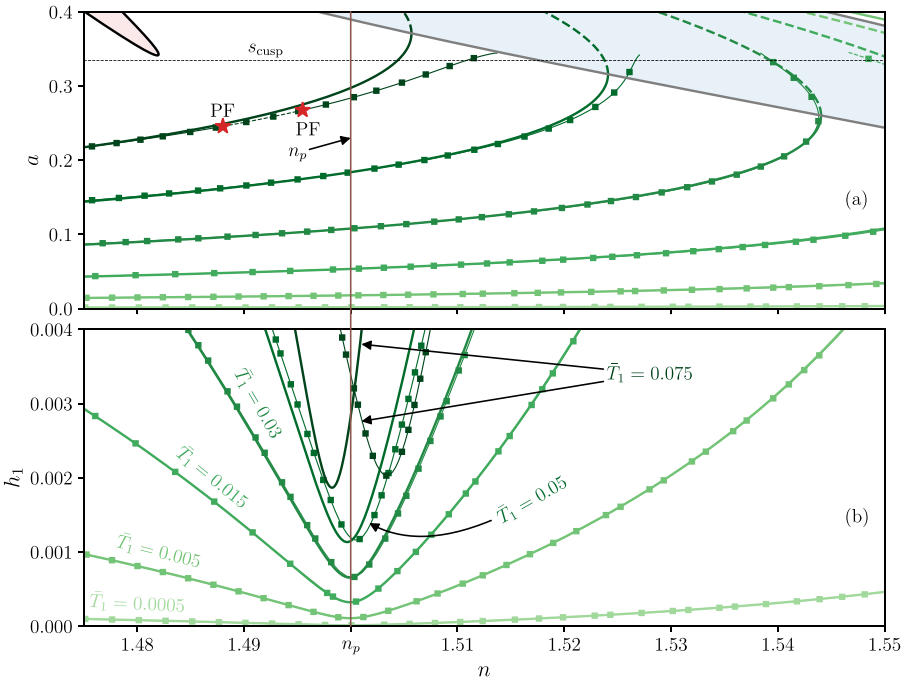

Fig. 5. Order response of the pendulums (a) and the rotor (b) for several torque amplitudes. The pendulums are tuned to lock the antiresonance at n_p. The unison response is represented in green and its unstable parts are dashed. The darker the line the larger the torque amplitude. The red and blue areas are the instability regions related to localisation and jumps, respectively. MANLAB solutions are represented as thin lines with square markers. The red stars indicate the pitchfork bifurcations obtained with MANLAB. The vertical brown line indicates n_p. $\bar{T}_1 = \{0.0005, 0.005, 0.015, 0.03, 0.05, 0.075\}$ and the other parameters are given in Table 1 except for $x_{[4]} = 0.3261$. (For interpretation of the references to colour in this figure legend, the reader is referred to the web version of this article.)

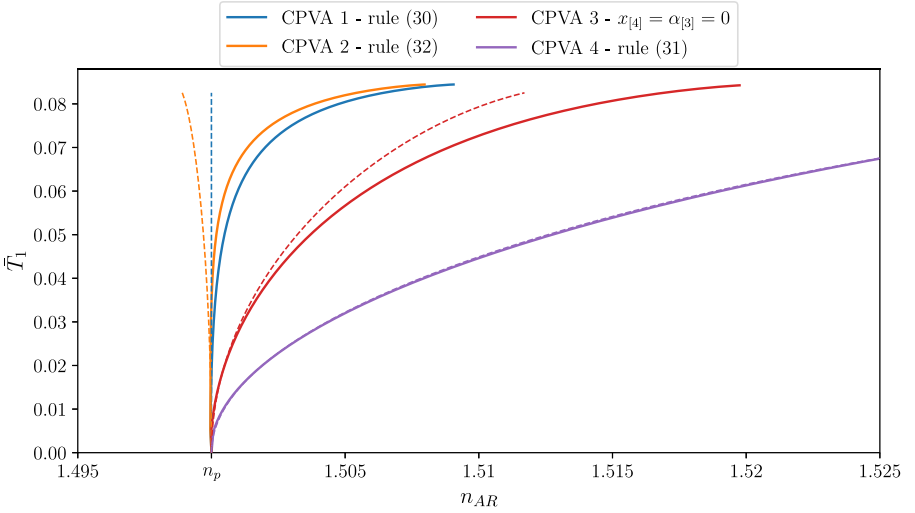

Fig. 6. Evolution of the antiresonance order as a function of the torque amplitude for four different designs. The parameters of the three CPVAs are given in Table 1 expect for $x_{[4]} = \{0.3261, 0.3460, 0, -0.5119\}$ for CPVAs 1, 2, 3 and 4, respectively, and $\alpha_{[3]} = 0$ for CPVA 3. The dashed lines represent the analytical approximation of n_{AR} obtained using Eq. (29), while the solid lines correspond to the antiresonance continuation procedure implemented in MANLAB [58].

Another rule limiting the shifting of the antiresonance was proposed by A. Renault [31–33]. It is derived from a regular perturbation solution of Eqs. (5a) and (5b) without damping, as presented in Appendix E, and leads to the recommendation

$$c_p = \frac{3\Lambda_m}{3(1+\mu)\Lambda_m - 4\mu\Lambda_c^2} c_c. \tag{32}$$

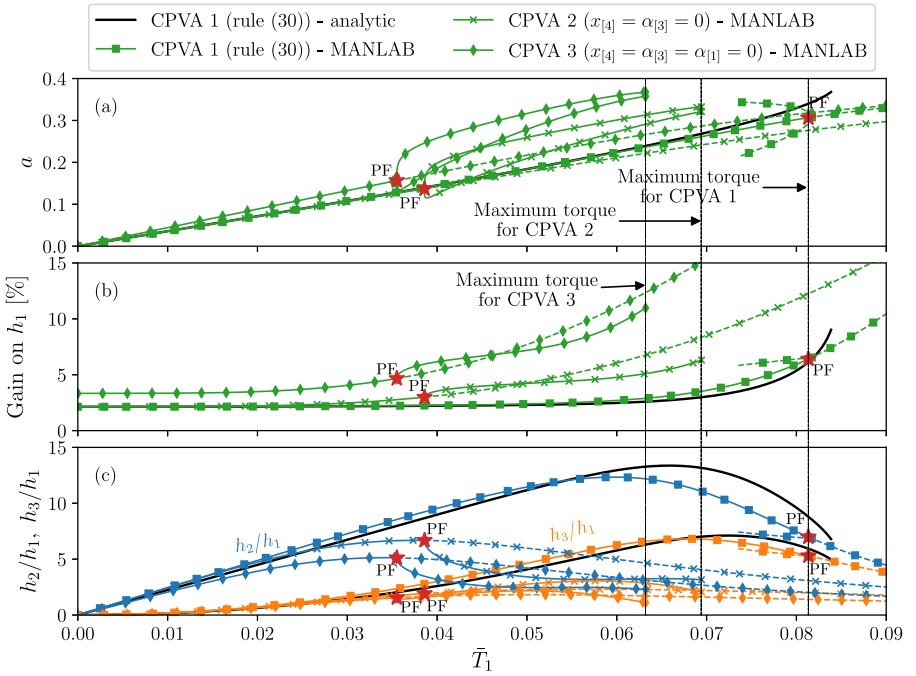

Fig. 7. Torque response of three different CPVAs at $n = n_p$. The solutions associated to the first, second and third CPVAs are shown as lines with square, cross and diamond markers, respectively. The first harmonic of the pendulums is shown in (a), the gain on the first harmonic of the rotor is shown in (b), and higher rotor harmonics are shown in (c). The gain shown in (b) is defined as $h_1/\bar{T}_1$, as the amplitude of the rotor with fixed pendulums is $\bar{T}_1$. Analytical results are shown in black for CPVA 1 (they are not shown for CPVAs 2 and 3 for clarity). Pitchfork bifurcations are indicated as red stars. Dashed lines indicate unstable solutions. The parameters of the three CPVAs are given in Table 1 expect for $x_{[4]} = \{0.3261, 0, 0\}$, $\alpha_{[3]} = \{-0.1, 0, 0\}$ and $\alpha_{[1]} = \{0.5, 0.5, 0\}$ for CPVAs 1, 2 and 3, respectively.

It is interesting to note that the design rule (30) is the same as Eq. (32) where the contribution of μ is neglected. These two rules are compared by computing the antiresonance order as a function of the excitation amplitude, as shown in Fig. 6. This computation is performed using MANLAB together with an antiresonance continuation procedure [58]. For comparison purposes, Fig. 6 also represents $n_{AR}(\bar{T}_1)$ for a CPVA tuned accordingly to rule (31) and for a reference CPVA for which no nonlinear mistuning is introduced (i.e. $x_{[4]} = \alpha_{[3]} = 0$, so that the rotation law is linear and the pendulums follow an epicycloidal path). We can see that rules (30) and (32) both limit efficiently the shifting of the antiresonance. Rule (32) is slightly more effective as it is the one keeping n_{AR} closest from n_p. In the case of the CPVA with no nonlinear mistuning, the antiresonance is largely shifting to the right, which shows that the antiresonance naturally has a hardening behaviour. The case of the CPVA with pendulums following the tautochronic path of the coupled system leads to the worst results. This is logical as the antiresonance is initially shifting to the right, and rule (31) increases even more this hardening behaviour. The analytical prediction of n_{AR} fits well with the numerical results for small torque amplitudes (around $\bar{T}_1 = 0.03$). For larger amplitudes the differences become significant, especially for designs that limit well the shifting of the antiresonance.

A torque response at $n = n_p$ of three different CPVAs is shown in Fig. 7.

- CPVA 1 is tuned using rule (30),
- The pendulums of CPVA 2 follow an epicycloid and a linear rotation law,
- The pendulums of CPVA 3 follow an epicycloid and do not rotate.

Note that no CPVA tuned accordingly to rule (32) is shown as it results in a response very close from that of CPVA 1 and the stability information is not provided by the analytical procedure detailed in Appendix E. The torque for which the pendulums reach their cusp is indicated for the three CPVAs. The pendulums of CPVA 3 cannot filter-out large torque amplitudes because localisation leads to a significant increase in amplitude, brining one of the pendulums to its cusp at $\bar{T}_1 \approx 0.0632$. A similar situation occurs for CPVA 2, with one of the pendulums reaching its cusp at $\bar{T}_1 \approx 0.0693$. The torque range of CPVA 1 is much larger than that of CPVAs 2 and 3. It is limited by the appearance of a subcritical pitchfork bifurcation, leading to a jump of the pendulums that brings them to their cusp. At small torque amplitudes, the gain on h_1 is the same for CPVAs 1 and 2, but it is larger for CPVA 3. This highlights the benefit of the added rotational motion of the pendulums. Starting from $\bar{T}_1 \approx 0.0265$, the gain for CPVAs 2 and 3 increases significantly compared to that of CPVA 1. In spite of the pendulums responding on a localised solution starting from $\bar{T}_1 = 0.0385$, CPVA 2 leads to a satisfying vibration reduction, with a gain of 6.4% when the pendulums reach their cusp. Still, one should be careful about the localised solution since a larger number of pendulums would likely reduce even more the torque

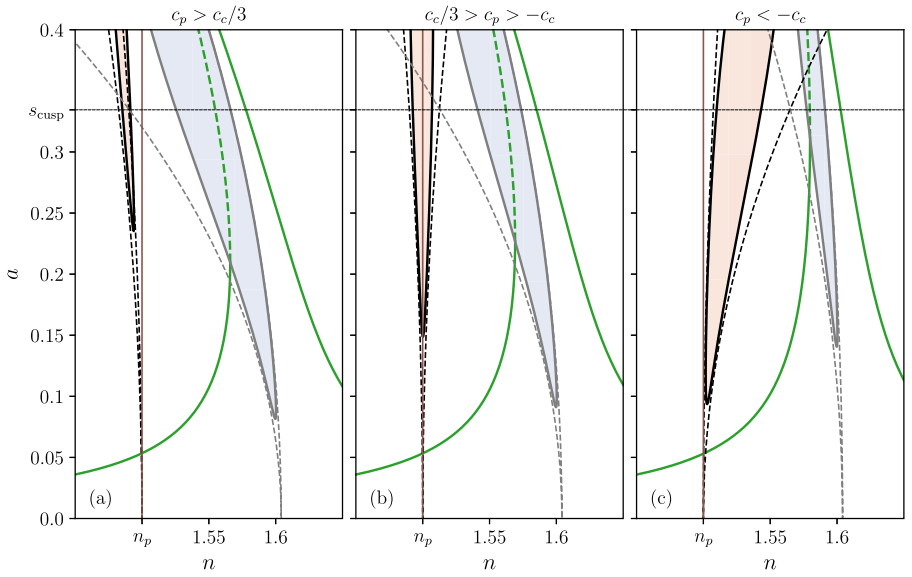

Fig. 8. Order response of the pendulums for three different values of nonlinear tuning. The unison response is represented in green and its unstable parts are dashed. The red and blue areas are the instability regions related to localisation and jumps, respectively. The dashed black and grey lines are 2nd order approximations of the limits of those regions in the conservative case. The vertical brown line indicates n_p. $\bar{T}_1 = 0.015$ and $x_{[4]} = \{0.25, 0.1, -0.25\}$ in (a), (b) and (c), respectively, while the other parameters are given in Table 1. (For interpretation of the references to colour in this figure legend, the reader is referred to the web version of this article.)

range [11]. The filtering with CPVA 3 is rather poor, with a gain exceeding 10% starting from as soon as $\bar{T}_1 = 0.0610$. Despite the small shift of the antiresonance visible in Figs. 5(b) and 6, the filtering of the 1st harmonic is extremely satisfying with CPVA 1. Indeed, Fig. 7(b) shows that the gain on most of the torque range is of 2.4%, and it does not exceed 6.4%. Though the pendulums are efficient in filtering the harmonic excitation, they generate higher rotor harmonics. Fig. 7(c) shows that this effect is absolutely not negligible as the amplitude of the 2nd and 3rd harmonics equals up to 12.4 and 7 times h_1, respectively, for CPVA 1. This issue is less visible for CPVAs 2 and 3, mostly because h_1 is larger. A possibility to limit the apparition of higher harmonics is to use pendulums tuned at different orders [14]. Another solution is to use another filtering principle of the CPVA, based on a subharmonic response [49,50,69]. Finally, the analytical model predicts accurately most of the response even though it indicates a shifting of the antiresonance in the wrong direction (*cf.* Fig. 5(b)). This is because the shifting predicted by the analytical model is roughly the opposite of the actual shifting.

4.3. Avoidance of the instabilities

As explained in Section 1, instabilities of the unison solution are to be avoided as they reduce the torque range of the CPVA and might decrease the vibration reduction. Hence, it is interesting to have a simple information on the position of the instability zones to know how to avoid them. This can be done by neglecting the damping and using Taylor series in a in the expression of $\sigma_{sn}(a)$ and $\sigma_{pf}(a)$, leading to

$$\sigma_{sn} = \frac{\Lambda_c^2 \tilde{\mu} n_p}{2\Lambda_m} + \frac{-2c_2 \pm c_2}{4\Lambda_m n_p} a^2 + \mathcal{O}(a^4), \tag{33a}$$

$$\sigma_{pf} = \frac{-2c_p \pm |c_2 - 2c_t|}{4\Lambda_m n_p} a^2 + \mathcal{O}(a^4) = \frac{-2c_p \pm |c_p - c_c|}{4\Lambda_m n_p} a^2 + \mathcal{O}(a^4) \tag{33b}$$

There are important remarks to be done about Eqs. (33a) and (33b):

- The bifurcation curve related to saddle-node bifurcations emanates from $\sigma = \Lambda_c^2 \tilde{\mu} n_p / 2\Lambda_m$, which corresponds to $n = n_{20} > n_p$. However, the bifurcation curve related to pitchfork bifurcations emanates from $\sigma = 0$, which corresponds to $n = n_p$.
- σ_{sn} increases with the amplitude if $c_2 < 0$ and decreases if $c_2 > 0$. It is logical that this bifurcation curve follows the sign of c_2 as jumps are due to the hardening/softening behaviour, and c_2 is the parameter that controls this behaviour (*cf.* Eq. (21)).
- σ_{pf} increases with the amplitude if $-2c_p - |c_p - c_c| > 0$ and decreases if $-2c_p + |c_p - c_c| < 0$. The case $-2c_p - |c_p - c_c| < 0 < -2c_p + |c_p - c_c|$ is highly undesired as σ_{pf} would remain around 0, causing the instability zone to exist at the operating point $n \approx n_p$. This is illustrated in Fig. 8.

In order to avoid instabilities while keeping $n_p \approx n$, the best options are to choose

$$2c_p > |c_p - c_c| \Leftrightarrow c_p > c_c/3 \text{ and } n_p < n, \text{ or} \tag{34a}$$

$$2c_p < -|c_p - c_c| \Leftrightarrow c_p < -c_c \text{ and } n_p > n. \tag{34b}$$

Conditions (34a) and (34b) correspond to the part of Fig. 8(a) where $n > n_p$ and to the part of Fig. 8(c) where $n < n_p$, respectively. Because of damping, the localisation zone does not start from $n = n_p$, so one can still use conditions (34a) and (34b) with $n_p = n$. In [29], linear over-tuning together with a hardening behaviour was recommended to avoid localisation. This is in agreement with condition (34b). In [8], which considered purely translated pendulums, it was proposed to use an over-tuned epicycloidal trajectory in order to keep the unison solution stable. The disadvantage of this method is that the level of detuning must be chosen depending on the maximum pendulums' amplitude desired, whereas conditions (34) prevent the appearance of a localised solution no matter the pendulums' amplitude. Moreover, the linear over-tuning required in [8] is relatively large, which decreases the efficiency of the vibration reduction (*cf.* Section 4.2). Finally, note that in the special case $c_p = c_c$ (which is recommended to keep the antiresonance locked, *cf.* Section 4.2), condition (34a) can be satisfied but not condition (34b). Hence, recommendation (34a) is compatible with recommendations (30) and (32).

In order to avoid the jumps up to the cusp, one must ensure that

$$\sigma < \min[\sigma_{sn}(s_{\text{cusp}})]. \tag{35}$$

4.4. Visualisation of the preferred design in the design space

Fig. 9 represents the stability of the unison solution at a given excitation order and as a function of the linear and nonlinear tuning parameters, n_p and $\bar{c}_p$, where the later is simply the unscaled version of c_p, i.e.

$$\bar{c}_p = 3(x_{[4]} + 2n_p^2 \eta \alpha_{[1]} \alpha_{[3]}). \tag{36}$$

For convenience, we also introduce the unscaled coefficient $\bar{c}_c = \mu n_t^4$. Fig. 9 contains four maps, all corresponding to a different pendulums' amplitude. Each set $(n_p, \bar{c}_p)$ corresponds to a given design, making the maps useful to assess simultaneously the stability of different designs. The designs subjected to jumps (localisation) at amplitude a are shown in blue (red). The stable designs are shown in green. The guidelines limiting the shifting of the antiresonance (30) and preventing the appearance of localisation (34) are also represented, so one can see the designs that allow performance and stability. The hatched areas indicate the designs for which the pendulums have reached their cusp, so the instability zones should be avoided until the design becomes hatched. The black dot corresponds to the design presented in Figs. 5 and 7 (CPVA 1 in Fig. 7).

The designs leading to the best vibration reduction are those located around the brown line and close to $n_p = n$. Fig. 9 shows that a small over-tuning could lead to localisation while a small under-tuning might cause a jump. Moreover, as explained in Section 4.3, the lower the damping the closer the instability zone is from n_p. Hence, to have an efficient and robust CPVA, the best choice is to choose $\bar{c}_p \approx \bar{c}_c$ and n_p equal or very slightly smaller than n.

5. Conclusion

This paper deals with the filtering efficiency of CPVAs and their dynamic stability. To consider modern CPVA designs, the N identical pendulums are allowed to rotate relatively to the rotor. The dynamic response of the system and its stability are computed using a perturbation method, and the validity of this analytical model is validated through comparisons with numerical solutions. Because the system is nonlinear, the resonance and antiresonance orders can increase/decrease with the excitation amplitude. We showed that in the case of pendulums following an epicycloidal path and a linear rotation law, the resonance order tends to diminish with the exciting torque amplitude, revealing a softening behaviour. This softening is due to nonlinearities arising through the coupling between the rotor and the pendulums. However, contrarily to the resonance, the antiresonance order increases with the excitation amplitude. Hence, to design an efficient CPVA, it is not sufficient to assess only the behaviour of the pendulums, which does not contain information regarding the evolution of the antiresonance order. In this paper, we derived design guidelines that allow to minimise the shifting of the antiresonance, thus leading to a maximised filtering over the whole torque range. These guidelines require the use of paths/rotation laws that slightly soften the system's response compared to the case of an epicycloid and a linear rotation. The accuracy of these guidelines was assessed using an antiresonance tracking procedure and a torque sweep confirmed the efficiency of such nonlinear tunings. This torque sweep also highlighted that the amplitude of higher rotor harmonics is not negligible at the operating point. Then, two other design guidelines preventing the apparition of localised solutions were proposed. One of them is highly relevant as it is compatible with the rule locking the antiresonance. Finally, a representation of the stability and design rules in the design space allowed to identify the CPVA tuning parameters leading to a stable response and a maximum vibration reduction.

CRediT authorship contribution statement

V. Mahé: Formal analysis, Investigation, Validation, Writing – original draft, Investigation, Methodology, Conceptualisation, Software. **A. Renault:** Supervision, Conceptualisation, Resources, Software. **A. Grolet:** Supervision, Validation, Visualisation. **H. Mahé:** Supervision. **O. Thomas:** Supervision, Validation, Visualisation, Writing – review & editing.

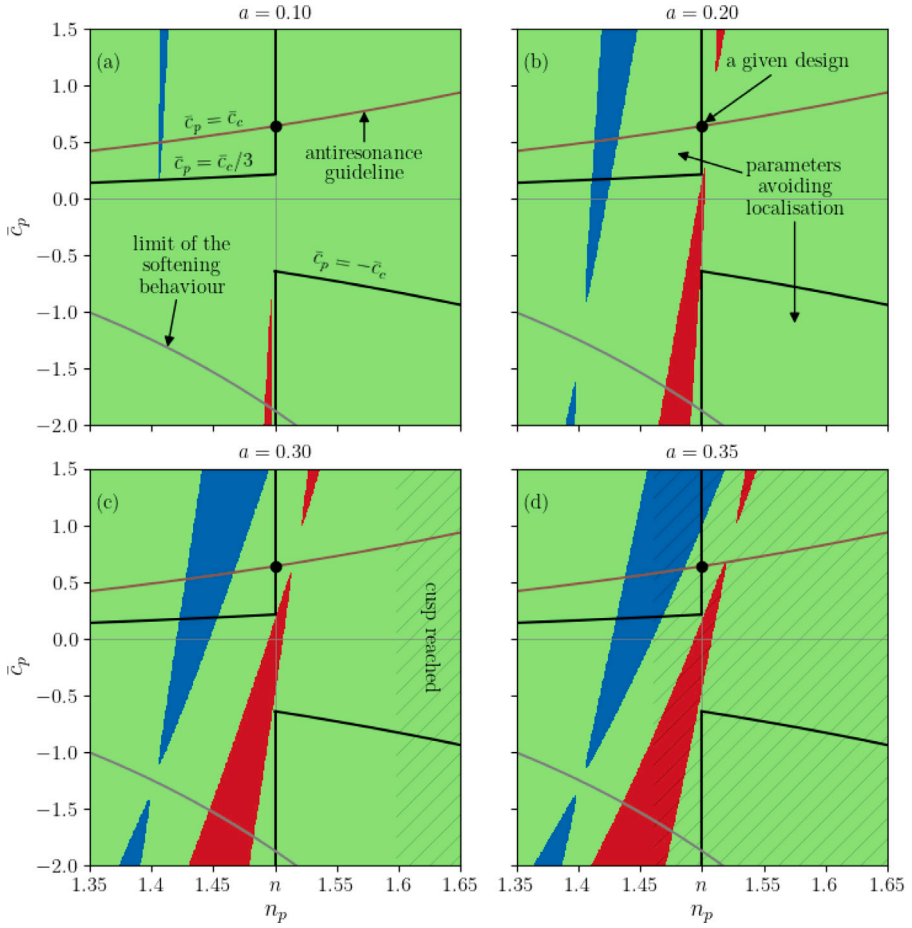

Fig. 9. Maps representing the stability of the response as a function of the tuning parameters n_p and $\bar{c}_p$. Each map is shown for a given order n and a given pendulums' amplitude a. Stable designs are depicted in green while designs subjected to localisation or jumps are shown in red or blue, respectively. The parameters avoiding localisation are delimited by black lines. The brown line corresponds to recommendation (30), locking the antiresonance. The grey line shows the limit between the hardening and softening behaviour of the unison mode. Designs below this line are hardening. The hatched areas indicate the designs for which amplitude a is larger than s_{cusp}. $n = 1.5$ and the parameters that are not varied are given in Table 1. (For interpretation of the references to colour in this figure legend, the reader is referred to the web version of this article.)

Declaration of competing interest

The authors declare that they have no known competing financial interests or personal relationships that could have appeared to influence the work reported in this paper.

Appendix A. System obtained through the method of multiple scales

The system of equations obtained through the application of the method of multiple scales is given by Eq. (17) where functions f_{a_i} and f_{ξ_i} are

$$f_{a_i}(\boldsymbol{a},\boldsymbol{\xi}) = \left[-2n_p\tilde{b}a_i + \frac{2\Lambda_c^2 n_p^2\tilde{\mu}}{N}\sum_{j=1}^{N} a_j \sin(\Delta\xi_{ij}) + \frac{1}{N}\sum_{j=1}^{N}\left[c_c a_i a_j^2 \sin(2\Delta\xi_{ij}) - \frac{c_t}{2}(a_j^3 + a_j a_i^2)\sin(\Delta\xi_{ij})\right] - \left(2\Lambda_c - \frac{c_f}{4}a_i^2\right)\tilde{T}_1 \sin(\xi_i)\right] \left[4\Lambda_m n_p\right]^{-1}, \tag{A.1}$$

$$f_{\xi_i}(\boldsymbol{a},\boldsymbol{\xi}) = \sigma a_i - \left[\frac{2\Lambda_c^2 n_p^2\tilde{\mu}}{N}\sum_{j=1}^{N} a_j \cos(\Delta\xi_{ij}) - c_p a_i^3 + \frac{1}{N}\sum_{j=1}^{N}\left[c_c a_i a_j^2 \cos(2\Delta\xi_{ij}) - \frac{c_t}{2}(a_j^3 + 3a_j a_i^2)\cos(\Delta\xi_{ij})\right] + \left(2\Lambda_c - \frac{3c_f}{4}a_i^2\right)\tilde{T}_1 \cos(\xi_i)\right] \left[4\Lambda_m n_p\right]^{-1}. \tag{A.2}$$

Constants c_p, c_c, c_t and c_f are defined in Eqs. (20) and (27) and $\Delta\xi_{ij}$ is defined as

$$\Delta\xi_{ij} = \xi_j - \xi_i. \tag{A.3}$$

Appendix B. Response of the systems with pendulums at unison

The amplitude and phase response of the pendulums at unison is given by

$$\sigma = \frac{2\Lambda_c^2 n_p^2 \tilde{\mu} - c_2 a^2}{4\Lambda_m n_p} \pm \frac{8\Lambda_c - 3c_f a^2}{16\Lambda_m n_p} \sqrt{\frac{\bar{T}_1^2}{a^2} - \frac{64 n_p^2 \tilde{b}^2}{(8\Lambda_c - c_f a^2)^2}}, \tag{B.1a}$$

$$\bar{T}_1 = 4a \left[\frac{\left(2n_p(2\Lambda_m\sigma - \Lambda_c^2 n_p \tilde{\mu}) + c_2 a^2\right)^2}{\left(8\Lambda_c - 3c_f a^2\right)^2} + \frac{4n_p^2 \tilde{b}^2}{\left(8\Lambda_c - c_f a^2\right)^2} \right]^{1/2}, \tag{B.1b}$$

$$\tan(\xi) = -\frac{2n_p \tilde{b}}{4\Lambda_m n_p \sigma - 2\Lambda_c^2 n_p^2 \tilde{\mu} + c_2 a^2} \frac{8\Lambda_c - 3c_f a^2}{8\Lambda_c - c_f a^2}. \tag{B.1c}$$

Eqs. (B.1a) and (B.1b) are used to compute the amplitude response as a function of the excitation order and excitation amplitude, respectively.

The rotor's response can be approximated by Eq. (24). The amplitudes h_i and phases ψ_i $(i = 1, 2, 3)$ of its harmonics are given by

$$h_1^2 = \bar{T}_1^2 + \mu \bar{T}_1 a \cos(\xi) \left(2n_p^2 \Lambda_c + \frac{n_t^2(1+n_t^2)}{4}(2n^2 - 3n_p^2)a^2 \right) + \frac{\mu^2 a^2}{4} \left(2n_p^2 \Lambda_c + \frac{n_t^2(1+n_t^2)}{4}(2n^2 - 3n_p^2)a^2 \right)^2, \tag{B.2a}$$

$$\tan(\psi_1) = \frac{\mu a \left(8n_p^2 \Lambda_c + n_t^2(1+n_t^2)(2n^2 - 3n_p^2)a^2 \right) \sin(\xi)}{\mu a \left(8n_p^2 \Lambda_c + n_t^2(1+n_t^2)(2n^2 - 3n_p^2)a^2 \right) \cos(\xi) + 8\bar{T}_1}, \tag{B.2b}$$

$$h_2 = \mu n n_t^2 a^2, \tag{B.2c}$$

$$\tan(\psi_2) = \frac{-\cos(2\xi)}{\sin(2\xi)}, \tag{B.2d}$$

$$h_3 = \frac{n_t^2(1+n_t^2)}{8}(n_p^2 + 2n^2)\mu a^3, \tag{B.2e}$$

$$\tan(\psi_3) = \frac{-\sin(3\xi)}{-\cos(3\xi)}. \tag{B.2f}$$

Appendix C. Expression of the bifurcation curves

The bifurcation curves $a_{sn}(\sigma)$ and $a_{pf}(\sigma)$ can be written as $\sigma_{sn}(a)$ and $\sigma_{pf}(a)$ such that

$$\sigma_{sn} = \frac{1}{4\Lambda_m n_p (8\Lambda_c + 3c_f a^2)} \left[\varpi_{sn_1} \pm \frac{\sqrt{\varpi_{sn_2}}}{(-8\Lambda_c + c_f a^2)^3} \right], \tag{C.1a}$$

$$\sigma_{pf} = \frac{1}{4\Lambda_m n_p (8\Lambda_c + 3c_f a^2)(-8\Lambda_c + c_f a^2)} \left[\varpi_{pf_1} \pm \frac{\sqrt{\varpi_{pf_2}}}{(-8\Lambda_c + c_f a^2)^2} \right], \tag{C.1b}$$

with

$$\varpi_{sn_1} = 12\Lambda_c c_t a^2 + 16\Lambda_c(\Lambda_c^2 n_p^2 \tilde{\mu} - c_2 a^2), \tag{C.2a}$$

$$\begin{aligned} \varpi_{sn_2} = {} & (-8\Lambda_c + c_f a^2)^3 (-8\Lambda_c + 3c_f a^2)^2 \Big[c_f a^2 \Big(-4n_p^2 \tilde{b}^2 (9c_f (8\Lambda_c + c_f a^2) a^2 - 64\Lambda_c^2) \\ & + c_2^2 a^4 \left((-24\Lambda_c + c_f a^2) c_f a^2 + 192\Lambda_c^2 \right) \Big) + 512\Lambda_c^3 (2n_p \tilde{b} + c_2 a^2)(2n_p \tilde{b} - c_2 a^2) \Big], \end{aligned} \tag{C.2b}$$

$$\varpi_{pf_1} = -c_f \left(6c_f c_c a^6 + 16\Lambda_c (c_t + 2c_p - c_2) a^4 \right) + 128\Lambda_c^2 c_p a^2, \tag{C.2c}$$

$$\begin{aligned} \varpi_{pf_2} = {} & (-8\Lambda_c + c_f a^2)^3 (-8\Lambda_c + 3c_f a^2)^2 \\ & \Big[c_f a^2 \Big[c_f a^2 \Big[c_f a^2 \left((3c_c - c_t + c_p)^2 a^4 - 36 n_p^2 \tilde{b}^2 \right) - 8\Lambda_c (36 n_p^2 \tilde{b}^2 + (c_c - c_t + 3c_p)(3c_c - c_t + c_p) a^4) \Big] \\ & - 64\Lambda_c^2 \left(-4n_p^2 \tilde{b}^2 + (9c_c c_t - 5c_c c_2 - 2c_t^2 + 7c_t c_p + c_t c_2 - 3c_p c_2) a^4 \right) \Big] - 512\Lambda_c^3 (2c_t - c_2)^2 a^4 + 2048\Lambda_c^3 n_p^2 \tilde{b}^2 \Big]. \end{aligned} \tag{C.2d}$$

Appendix D. Study of the uncoupled system

In this section, we focus on the case of where no fluctuating torque is applied on the rotor so that is spins at a constant speed. Hence, it is not a degree-of-freedom and the pendulums are uncoupled from the rotor. Setting $y = 1, y' = 0$ in Eq. (5b) and ignoring the damping leads to

$$\left[1 + \eta\gamma(s_i)^2\right] s_i'' + \eta\gamma(s_i)\frac{d\gamma(s_i)}{ds_i} s_i'^2 - \frac{1}{2}\frac{dx(s_i)}{ds_i} = 0, \qquad i = 1, \dots, N. \tag{D.1}$$

Considering that the paths and rotation functions are given by Eq. (10), Eq. (D.1) can be rewritten as

$$\Lambda_m s_i'' + n_t^2 s_i - 2x_{[4]} s_i^3 + 6\eta\alpha_{[1]}\alpha_{[3]}\left(s_i^2 s_i'' + s_i s_i'^2\right) + 9\eta\alpha_{[3]}^2\left(s_i^4 s_i'' + 2s_i^3 s_i'^2\right) = 0, \qquad i = 1, \dots, N. \tag{D.2}$$

In the special case $x_{[4]} = \alpha_{[3]} = 0$, Eq. (D.2) becomes a linear equation, meaning that the configuration $x_{[4]} = \alpha_{[3]} = 0$ yields a tautochronic behaviour of the pendulums. In the following, we look for other sets $(x_{[4]}, \alpha_{[3]})$ that approximately lead to a tautochronic behaviour. Like in Section 3, this is done using the scaling $x_{[4]} = \epsilon\tilde{x}_{[4]}$, $\alpha_{[3]} = \epsilon\tilde{\alpha}_{[3]}$ and the method of multiple scales with the fast time $\vartheta_0 = \vartheta$ and the slow one $\vartheta_1 = \epsilon\vartheta$. Using the expansion (14) and the steady state condition (18), one finds that the backbone curve of the ith uncoupled pendulum is

$$n_{uc} = n_p - \frac{c_p}{4\Lambda_m n_p} a^2. \tag{D.3}$$

Hence, for the period of oscillation of the pendulums to be independent on their amplitude, one must have

$$c_p = 0. \tag{D.4}$$

Note that Eq. (D.3) can also be retrieved by setting $\mu = 0$ in the backbone curve of the unison mode (21).

Appendix E. Application of a regular perturbation method on the equations of motion

Here we present the application of a regular perturbation method on Eqs. (5a) and (5b) without damping. Only one pendulum is considered, but the procedure is exactly the same with N pendulums. First, variables y and s are expanded such that

$$s = \epsilon s_1 + \epsilon^2 s_2 + \epsilon^3 s_3 + \mathcal{O}(\epsilon^4), \tag{E.1a}$$

$$y = 1 + \epsilon y_{\theta 1} + \epsilon^2 y_{\theta 2} + \epsilon^3 y_{\theta 3} + \mathcal{O}(\epsilon^4). \tag{E.1b}$$

Note that because damping is neglected, the constant part of the torque must not be considered. Indeed, in practice it balances with the rotor's damping such that $\bar{b}_r = \bar{T}_0$ (*cf.* Section 2.1). Introducing the expansions in the equations of motion leads to three systems of two equations, the ith system appearing at order ϵ^i. These systems are given by

$$\begin{cases} (1+\mu) y_{\theta 1}' + \mu\Lambda_c s_1'' &= \bar{T}_1 \cos(n\vartheta), \quad \text{(a)} \\ \Lambda_c y_{\theta 1}' + \Lambda_m s_1'' + n_t^2 s_1 &= 0 \quad \text{(b)} \end{cases}$$
$$\begin{cases} (1+\mu) y_{\theta 2}' + \mu\Lambda_c s_2'' &= f_{\theta 2}(y_{\theta 1}, s_1), \quad \text{(c)} \\ \Lambda_c y_{\theta 2}' + \Lambda_m s_2'' + n_t^2 s_2 &= f_{s2}(y_{\theta 1}, s_1), \quad \text{(d)} \end{cases} \tag{E.2}$$
$$\begin{cases} (1+\mu) y_{\theta 3}' + \mu\Lambda_c s_3'' &= f_{\theta 3}(y_{\theta 1}, s_1, y_{\theta 2}, s_2), \quad \text{(e)} \\ \Lambda_c y_{\theta 3}' + \Lambda_m s_3'' + n_t^2 s_3 &= f_{s3}(y_{\theta 1}, s_1, y_{\theta 2}, s_2), \quad \text{(f)} \end{cases}$$

with

$$f_{\theta 2}(y_{\theta 1}, s_1) = -\mu[\Lambda_c y_{\theta 1}' s_1' - 2n_t^2 s_1 s_1' + (2\Lambda_c s_1'' + y_{\theta 1}') y_{\theta 1}] - y_{\theta 1} y_{\theta 1}', \tag{E.3a}$$

$$f_{s2}(y_{\theta 1}, s_1) = -\Lambda_m (y_{\theta 1}' s_1' + y_{\theta 1} s_1'') - n_t^2 y_{\theta 1} s_1 \tag{E.3b}$$

$$\begin{aligned} f_{\theta 3}(y_{\theta 1}, s_1, y_{\theta 2}, s_2) = -\mu \Bigg[& \left(\Lambda_c y_{\theta 1}^2 + 2\Lambda_c y_{\theta 2}\right) s_1'' + \left(\Lambda_c y_{\theta 2}' - 2n_t^2 s_2\right) s_1' + \left(3\alpha_{[3]}\eta s_1'' - \frac{n_t^2(1+n_t^2)}{2} s_1''\right) s_1^2 \\ & + \left(\Lambda_c s_2' - n_t^2 s_1^2 + y_{\theta 2}\right) y_{\theta 1}' + \left(6\alpha_{[3]}\eta s_1'^2 - n_t^2(1+n_t^2) s_1'^2 - 2n_t^2 s_2'\right) s_1 \\ & + \left(2\Lambda_c s_2'' - 4n_t^2 s_1 s_1' + \Lambda_c y_{\theta 1}' s_1' + y_{\theta 2}'\right) y_{\theta 1} \Bigg] - y_{\theta 1} y_{\theta 2}' - y_{\theta 2} y_{\theta 1}', \end{aligned} \tag{E.3c}$$

$$\begin{aligned} f_{s3}(y_{\theta 1}, s_1, y_{\theta 2}, s_2) = & -6\alpha_{[1]}\alpha_{[3]}\eta s_1^2 s_1'' + 2x_{[4]} s_1^3 - \Lambda_m y_{\theta 2} s_1'' - \Lambda_m y_{\theta 2}' s_1' - \left(6\alpha_{[1]}\alpha_{[3]}\eta s_1'^2 + n_t^2 y_{\theta 2}\right) s_1 \\ & - \left(\Lambda_m s_2' + \left(3\alpha_{[3]}\eta - \frac{n_t^2(1+n_t^2)}{2}\right) s_1^2\right) y_{\theta 1}' - \left(\Lambda_m s_2'' + n_t^2 s_2\right) y_{\theta 1}. \end{aligned} \tag{E.3d}$$

Looking at the nature of the forcing terms in the three systems of equations, it makes sense to look for solutions of the form

$$y_{\theta 1} = \Re[\hat{h}_{1(1)} e^{jn\vartheta}], \quad s_1 = \Re[\hat{a}_{1(1)} e^{jn\vartheta}], \tag{E.4a}$$

$$y_{\theta 2} = \Re[\hat{h}_{2(2)} e^{2jn\vartheta}], \quad s_2 = a_{2(0)} + \Re[\hat{a}_{2(2)} e^{2jn\vartheta}], \tag{E.4b}$$

$$y_{\theta 3} = \Re[\hat{h}_{3(1)} e^{jn\vartheta}] + \Re[\hat{h}_{3(3)} e^{3jn\vartheta}], \quad s_3 = \Re[\hat{a}_{3(1)} e^{jn\vartheta}] + \Re[\hat{a}_{3(3)} e^{3jn\vartheta}], \tag{E.4c}$$

where $\hat{\bullet}$ denotes a complex quantity and the index in brackets refers to the number of the harmonic. Inserting these general forms of solution in the three systems of equations and assuming $n = n_p$ leads to

$$\hat{h}_{1(1)} = 0, \quad \hat{a}_{1(1)} = -\frac{\bar{T}_1}{\mu \Lambda_c n_p^2}, \tag{E.5a}$$

$$\hat{h}_{2(2)} = \frac{3\mu \Lambda_m^2 n_p^2 \hat{a}_{1(1)}^2}{2(3(1+\mu)\Lambda_m) - 4\mu\Lambda_c^2}, \quad \hat{a}_{2(2)} = -j\frac{\mu \Lambda_m \Lambda_c n_p \hat{a}_{1(1)}^2}{3(1+\mu)\Lambda_m - 4\mu\Lambda_c^2}, \tag{E.5b}$$

$$\hat{h}_{3(1)} = j\frac{2n_p^3 \Lambda_m \hat{h}_{2(2)} - 3n_p(x_{[4]} + 2n_p^2 \eta \alpha_{[1]} \alpha_{[3]}) \hat{a}_{1(1)}^2}{2\Lambda_c n_p^2}. \tag{E.5c}$$

The expressions for $\hat{h}_{3(3)}$, $\hat{a}_{3(1)}$ and $\hat{a}_{3(3)}$ are not necessary to study the position of the antiresonance. As $\hat{h}_{1(1)} = 0$, the condition to lock the antiresonance at n_p is $\hat{h}_{3(1)} = 0$. Solving this leads to condition (32).

References

[1] B.C. Carter, Improvements in or relating to damping of oscillation-checking devices, 1929, 337 466.

[2] R.R.R. Sarazin, Means adapted to reduce the torsional oscillations of crankshafts, 1931, 2 079 226.

[3] R. Chilton, Pendulum counterweight, 1935, 2 112 984.

[4] M. Auleley, O. Thomas, C. Giraud-Audine, H. Mahé, Enhancement of a dynamic vibration absorber by means of an electromagnetic shunt, J. Intell. Mater. Syst. Struct. 32 (3) (2021) 331–354, http://dx.doi.org/10.1177/1045389X20957097.

[5] D.E. Newland, Nonlinear problems of centrifugal pendulum vibration absorbers, in: Mechanisms and Machines, Vol. 1, Varna (Bulgaria), 1965, pp. 39–62.

[6] J.F. Madden, Constant frequency bifilar vibration absorber, 1980, 4 218 187.

[7] H.H. Denman, Tautochronic bifilar pendulum torsion absorbers for reciprocating engines, J. Sound Vib. 159 (2) (1992) 251–277, http://dx.doi.org/10.1016/0022-460X(92)90035-V.

[8] S.W. Shaw, B. Geist, Tuning for performance and stability in systems of nearly tautochronic torsional vibration absorbers, J. Vib. Acoust. 132 (4) (2010) http://dx.doi.org/10.1115/1.4000840.

[9] A. Givois, J.-J. Tan, C. Touzé, O. Thomas, Backbone curves of coupled cubic oscillators in one-to-one internal resonance: Bifurcation scenario, measurements and parameter identification, Meccanica 55 (3) (2020) 481–503, http://dx.doi.org/10.1007/s11012-020-01132-2.

[10] A. Grolet, Z. Shami, S. Arabi, O. Thomas, Experimental nonlinear localisation in a system of two coupled beams, in: Dynamical System Theory and Applications, Lodz (Poland), 2019, p. 13.

[11] C.-P. Chao, C.-T. Lee, S. Shaw, Non-unisson dynamics of multiple centrifugal pendulum vibration absorbers, J. Sound Vib. 204 (5) (1997) 769–794, http://dx.doi.org/10.1006/jsvi.1997.0960.

[12] C.-P. Chao, S.W. Shaw, C.-T. Lee, Stability of the unison response for a rotating system with multiple tautochronic pendulum vibration absorbers, J. Appl. Mech. 64 (1) (1997) 149–156, http://dx.doi.org/10.1115/1.2787266.

[13] A. Alsuwaiyan, S.W. Shaw, Performance and dynamic stability of general-path centrifugal pendulum vibration absorbers, J. Sound Vib. 252 (5) (2002) 791–815, http://dx.doi.org/10.1006/jsvi.2000.3534.

[14] B.J. Vidmar, S.W. Shaw, B.F. Feeny, B.K. Geist, Nonlinear interactions in systems of multiple order centrifugal pendulum vibration absorbers, J. Vib. Acoust. 135 (6) (2013) http://dx.doi.org/10.1115/1.4024969.

[15] A.S. Alsuwaiyan, S.W. Shaw, Non-synchronous and localized responses of systems of identical centrifugal pendulum vibration absorbers, Arab. J. Sci. Eng. 39 (12) (2014) 9205–9217, http://dx.doi.org/10.1007/s13369-014-1464-1.

[16] J.S. Issa, S.W. Shaw, Synchronous and non-synchronous responses of systems with multiple identical nonlinear vibration absorbers, J. Sound Vib. 348 (2015) 105–125, http://dx.doi.org/10.1016/j.jsv.2015.03.021.

[17] A. Grolet, A. Renault, O. Thomas, Energy localisation in periodic structures: Application to centrifugal pendulum vibration absorber, in: International Symposium on Transport Phenomena and Dynamics of Rotating Machinery, Maui (Hawaii), 2017.

[18] K. Nishimura, T. Ikeda, Y. Harata, Localization phenomena in torsional rotating shaft systems with multiple centrifugal pendulum vibration absorbers, Nonlinear Dynam. 83 (3) (2016) 1705–1726, http://dx.doi.org/10.1007/s11071-015-2441-2.

[19] C.-T. Lee, S.W. Shaw, The non-linear dynamic response of paired centrifugal pendulum vibration absorbers, J. Sound Vib. 203 (5) (1997) 731–743, http://dx.doi.org/10.1006/jsvi.1996.0707.

[20] C.-T. Lee, S.W. Shaw, V.T. Coppola, A subharmonic vibration absorber for rotating machinery, J. Vib. Acoust. 119 (4) (1997) 590–595, http://dx.doi.org/10.1115/1.2889766.

[21] C.-P. Chao, S.W. Shaw, The effects of imperfections on the performance of the subharmonic vibration absorber system, J. Sound Vib. 215 (5) (1998) 1065–1099, http://dx.doi.org/10.1006/jsvi.1998.1634.

[22] C.-P. Chao, S.W. Shaw, The dynamic response of multiple pairs of subharmonic torsional vibration absorbers, J. Sound Vib. 231 (2) (2000) 411–431, http://dx.doi.org/10.1006/jsvi.1999.2722.

[23] Les amortisseurs dynamiques de vibrations [dynamic vibration dampers], Rev. Tech. Hispano Suiza (3) (1939).

[24] R. Chilton, Rocking dynamic damper, 1939, 2184734.

[25] R.W. Zdanowich, T.S. Wilson, The elements of pendulum dampers, Proc. Inst. Mech. Eng. 143 (1) (1940) 182–210, http://dx.doi.org/10.1243/PIME_PROC_1940_143_028_02.

[26] V. Mahe, A. Renault, A. Grolet, O. Thomas, H. Mahe, Dynamic stability of centrifugal pendulum vibration absorbers allowing a rotational mobility, J. Sound Vib. 517 (2022) 116525, http://dx.doi.org/10.1016/j.jsv.2021.116525.

[27] R.G. Mitchiner, R.G. Leonard, Centrifugal pendulum vibration absorbers—theory and practice, J. Vib. Acoust. 113 (4) (1991) 503–507, http://dx.doi.org/10.1115/1.2930214.

[28] J. Mayet, H. Ulbrich, Tautochronic centrifugal pendulum vibration absorbers: General design and analysis, J. Sound Vib. 333 (3) (2014) 711–729, http://dx.doi.org/10.1016/j.jsv.2013.09.042.
[29] J. Mayet, H. Ulbrich, First-order optimal linear and nonlinear detuning of centrifugal pendulum vibration absorbers, J. Sound Vib. 335 (2015) 34–54, http://dx.doi.org/10.1016/j.jsv.2014.09.017.
[30] J.A.C. Mayet, Centrifugal Vibration Absorbers: Theory and Application (Ph.D. thesis), Technische Universität München, München, 2015.
[31] A. Renault, Calcul et Optimisation d'Absorbeurs Pendulaires Dans une Chaîne de Traction Automobile [Simulation and Optimisation of Pendular Absorbers for Automotive Powertrain] (Ph.D. thesis), ENSAM, Lille, France, 2018.
[32] H. Mahé, A. Renault, O. Thomas, Dispositif d'amortissement pendulaire [pendular damping device], 2018, FR 3 055 038.
[33] H. Mahé, A. Renault, O. Thomas, Dispositif d'amortissement pendulaire [pendular damping device], 2018, FR 3 055 037.
[34] M.A. Acar, Design and Tuning of Centrifugal Pendulum Vibration Absorbers (Ph.D. thesis), Michigan State University, Michigan, 2017.
[35] M. Cirelli, J. Gregori, P. Valentini, E. Pennestrí, A design chart approach for the tuning of parallel and trapezoidal bifilar centrifugal pendulum, Mech. Mach. Theory 140 (2019) 711–729, http://dx.doi.org/10.1016/j.mechmachtheory.2019.06.030.
[36] M. Cirelli, M. Cera, E. Pennestrì, P.P. Valentini, Nonlinear design analysis of centrifugal pendulum vibration absorbers: An intrinsic geometry-based framework, Nonlinear Dynam. 102 (3) (2020) 1297–1318, http://dx.doi.org/10.1007/s11071-020-06035-1.
[37] M. Cera, M. Cirelli, E. Pennestrì, P. Valentini, The kinematics of curved profiles mating with a caged idle roller - higher-path curvature analysis, Mech. Mach. Theory 164 (2021) 104414, http://dx.doi.org/10.1016/j.mechmachtheory.2021.104414.
[38] M. Cera, M. Cirelli, E. Pennestrì, P.P. Valentini, Design analysis of torsichrone centrifugal pendulum vibration absorbers, Nonlinear Dynam. 104 (2) (2021) 1023–1041, http://dx.doi.org/10.1007/s11071-021-06345-y.
[39] M. Cera, M. Cirelli, E. Pennestrì, P.P. Valentini, Nonlinear dynamics of torsichrone CPVA with synchroringed form closure constraint, Nonlinear Dynam. (2021) http://dx.doi.org/10.1007/s11071-021-06732-5.
[40] X. Tan, S. Yang, J. Yang, J. Li, Study of dynamics of rotational centrifugal pendulum vibration absorbers based on tautochronic design, Meccanica (2021) http://dx.doi.org/10.1007/s11012-021-01340-4.
[41] E.R. Gomez, I.L. Arteaga, L. Kari, Normal-force dependant friction in centrifugal pendulum vibration absorbers: Simulation and experimental investigations, J. Sound Vib. 492 (2021) 115815, http://dx.doi.org/10.1016/j.jsv.2020.115815.
[42] E.R. Gomez, J. Sjöstrand, L. Kari, I.L. Arteaga, Torsional vibrations in heavy-truck powertrains with flywheel attached centrifugal pendulum vibration absorbers, Mech. Mach. Theory 167 (2022) 104547, http://dx.doi.org/10.1016/j.mechmachtheory.2021.104547.
[43] K. Kadoi, T. Inoue, J. Kawano, M. Kondo, Nonlinear analysis of a torsional vibration of a multidegrees-of-freedom system with centrifugal pendulum vibration absorbers and its suppression, J. Vib. Acoust. 140 (6) (2018) 061008, http://dx.doi.org/10.1115/1.4040042.
[44] C. Shi, R.G. Parker, Modal properties and stability of centrifugal pendulum vibration absorber systems with equally spaced, identical absorbers, J. Sound Vib. 331 (21) (2012) 4807–4824, http://dx.doi.org/10.1016/j.jsv.2012.05.018.
[45] C. Shi, R.G. Parker, Modal structure of centrifugal pendulum vibration absorber systems with multiple cyclically symmetric groups of absorbers, J. Sound Vib. 332 (18) (2013) 4339–4353, http://dx.doi.org/10.1016/j.jsv.2013.03.009.
[46] C. Shi, R.G. Parker, S.W. Shaw, Tuning of centrifugal pendulum vibration absorbers for translational and rotational vibration reduction, Mech. Mach. Theory 66 (2013) 56–65, http://dx.doi.org/10.1016/j.mechmachtheory.2013.03.004.
[47] C. Shi, R.G. Parker, Vibration modes and natural frequency veering in three-dimensional, cyclically symmetric centrifugal pendulum vibration absorber systems, J. Vib. Acoust. 136 (1) (2014) 011014, http://dx.doi.org/10.1115/1.4025678.
[48] C. Shi, S.W. Shaw, R.G. Parker, Vibration reduction in a tilting rotor using centrifugal pendulum vibration absorbers, J. Sound Vib. 385 (2016) 55–68, http://dx.doi.org/10.1016/j.jsv.2016.08.035.
[49] V. Mahe, A. Renault, A. Grolet, H. Mahe, O. Thomas, Subharmonic centrifugal pendulum vibration absorbers allowing a rotational mobility, Mech. Syst. Signal Process. 177 (2022) 109125, http://dx.doi.org/10.1016/j.ymssp.2022.109125.
[50] V. Mahé, A. Renault, A. Grolet, H. Mahe, O. Thomas, On the stability of pairs of subharmonic centrifugal pendulum vibration absorbers allowing a rotational mobility, Nonlinear Dyn. (2022) submitted for publication.
[51] V. Mahé, A. Renault, A. Grolet, H. Mahé, O. Thomas, Localised response of a centrifugal pendulum vibration absorber, Nonlinear Dyn. (2022) submitted for publication.
[52] J. Mayet, M.A. Acar, S.W. Shaw, Effective and robust rocking centrifugal pendulum vibration absorbers, J. Sound Vib. 527 (2022) 116821, http://dx.doi.org/10.1016/j.jsv.2022.116821.
[53] B. Geist, V. Ramakrishnan, P. Attibele, W. Resh, Precision requirements for the bifilar hinge slots of a centrifugal pendulum vibration absorber, Precis. Eng. 52 (2018) 1–14, http://dx.doi.org/10.1016/j.precisioneng.2017.08.001.
[54] V. Manchi, C. Sujatha, Torsional vibration reduction of rotating shafts for multiple orders using centrifugal double pendulum vibration absorber, Appl. Acoust. 174 (2021) 107768, http://dx.doi.org/10.1016/j.apacoust.2020.107768.
[55] D.E. Newland, Nonlinear aspects of the performance of centrifugal pendulum vibration absorbers, J. Eng. Ind. 86 (3) (1964) 257–263, http://dx.doi.org/10.1115/1.3670529.
[56] M. Sharif-Bakhtiar, S.W. Shaw, Effects of nonlinearities and damping on the dynamic response of a centrifugal pendulum vibration absorber, J. Vib. Acoust. 114 (3) (1992) 305–311, http://dx.doi.org/10.1115/1.2930262.
[57] A.G. Haddow, S.W. Shaw, Centrifugal pendulum vibration absorbers: An experimental and theoretical investigation, Nonlinear Dynam. 34 (3/4) (2003) 293–307, http://dx.doi.org/10.1023/B:NODY.0000013509.51299.c0.
[58] A. Renault, O. Thomas, H. Mahé, Numerical antiresonance continuation of structural systems, Mech. Syst. Signal Process. 116 (2019) 963–984, http://dx.doi.org/10.1016/j.ymssp.2018.07.005.
[59] S.W. Shaw, S. Wiggins, Chaotic dynamics of a whirling pendulum, Physica D 31 (2) (1988) 190–211, http://dx.doi.org/10.1016/0167-2789(88)90076-0.
[60] L. Shen, B.W. Suter, Bounds for eigenvalues of arrowhead matrices and their applications to hub matrices and wireless communications, EURASIP J. Adv. Signal Process. 2009 (1) (2009) 379402, http://dx.doi.org/10.1155/2009/379402.
[61] S.W. Shaw, M.A. Acar, B.F. Feeny, B.K. Geist, Modal properties of rotating shafts with order-tuned absorbers, in: J. De Clerck (Ed.), Topics in Modal Analysis I, Vol. 7, Springer International Publishing, Cham, 2014, pp. 181–189, http://dx.doi.org/10.1007/978-3-319-04753-9_18.
[62] M. Auleley, C. Giraud-Audine, H. Mahé, O. Thomas, Tunable electromagnetic resonant shunt using pulse-width modulation, J. Sound Vib. 500 (2021) 116018, http://dx.doi.org/10.1016/j.jsv.2021.116018.
[63] A.H. Nayfeh, Perturbation Methods, in: Wiley Classics Library, Wiley-VCH, Weinheim, 1973, http://dx.doi.org/10.1002/9783527617609.
[64] M. Golubitsky, I. Stewart, D.G. Schaeffer, in: J.E. Marsden, L. Sirovich (Eds.), Singularities and Groups in Bifurcation Theory, in: Applied Mathematical Sciences, vol. 2, Springer New York, New York, NY, 1988, http://dx.doi.org/10.1007/978-1-4612-4574-2.
[65] L. Guillot, A. Lazarus, O. Thomas, C. Vergez, B. Cochelin, A purely frequency based Floquet-Hill formulation for the efficient stability computation of periodic solutions of ordinary differential systems, J. Comput. Phys. 416 (2020) 109477, http://dx.doi.org/10.1016/j.jcp.2020.109477.
[66] L. Guillot, B. Cochelin, C. Vergez, A taylor series-based continuation method for solutions of dynamical systems, Nonlinear Dynam. 98 (4) (2019) 2827–2845, http://dx.doi.org/10.1007/s11071-019-04989-5.
[67] S.W. Shaw, P.M. Schmitz, A.G. Haddow, Tautochronic vibration absorbers for rotating systems, J. Comput. Nonlinear Dyn. 1 (4) (2006) 283–293, http://dx.doi.org/10.1115/1.2338652.
[68] R.J. Monroe, S.W. Shaw, A.H. Haddow, B.K. Geist, Accounting for roller dynamics in the design of bifilar torsional vibration absorbers, J. Vib. Acoust. 133 (6) (2011) http://dx.doi.org/10.1115/1.4003942.
[69] C.-T. Lee, S.W. Shaw, On the counteraction of periodic torques for rotating systems using centrifugally driven vibration absorbers, J. Sound Vib. 191 (5) (1996) 695–719, http://dx.doi.org/10.1006/jsvi.1996.0151.